From the holdings of the Department of Special Collections , Princeton University Library, Princeton, NJ

These documents are either in the public domain, or can only be used for educational and research purposes (Fair use) as per U.S. Copyright law (text below). By accessing this file, all users agree that their use falls in the public domain or within fair use as defined by the copyrightlaw. We do not charge any permission or usage fees for the publication of images of material inour collections, including those provided by Princeton University Library, via our website, catalog, or directly from staff.For more information regarding copyright, credit, and citation please review the information onthe Copyright, Credit and Citation Guidelines page of our website.
https://library.princeton.edu/special-collections/policies/copyright-credit-and-citation-guidelines. If you have any questions, including how to order higher-quality images from the collection, contact Special Collections Public Services via our Ask Us! Form. https://library.princeton.edu/special-collections/ask-us

---

Doctoral Dissertations, 2011-2026 Mathematics

2015

Geometry of (1,1)-Knots and Knot Floer Homology

Racz, Bela Andras

Princeton, NJ : Princeton University

---

http://arks.princeton.edu/ark:/88435/dsp01ft848s85j

U.S. Copyright law: The copyright law of the United States (Title 17, §108, United States Code) governs the making of photocopies or other reproductions of copyrighted material. Under certain conditions specified in the law, libraries and archives are authorized to furnish a photocopy or other reproduction. One of these specified conditions is that the photocopy or reproduction is not to be used for any purpose other than private study, scholarship, or research. If a user makes a request for, or later uses, a photocopy or reproduction for purposes in excess of fair use that user may be liable for copyright infringement. This institution reserves the right to refuse to accept a copying order if, in its judgment, fulfillment of the order would involve a violation of copyright law. https://www.copyright.gov/title17/title17.pdf

Geometry of (1,1)-Knots and Knot Floer Homology

Béla András Rácz

A Dissertation
Presented to the Faculty
of Princeton University
in Candidacy for the Degree
of Doctor of Philosophy

Recommended for Acceptance
by the Department of
Mathematics
Adviser: Zoltán Szabó

January 2015

© Copyright by Béla András Rácz, 2014.

All Rights Reserved

Abstract

We apply the technique of Heegaard Floer Homology to $(1,1)$-knots (1-bridge knots on the torus) to determine all $(1,1)$-knots of crossing number up to 12. We also prove miscellaneous results regarding (1,1)-knots, including the existence of a family with trivial Alexander polynomial, and symmetry results.

In addition, we define and study a new class of multi-pointed Heegaard diagrams for links in S^3 that generalizes the classical notion of grid diagrams.

Acknowledgements

I would like to thank my advisor Zoltán Szabó for introducing me to the fascinating world of knots, knot invariants, and many interesting problems in this field, as well as for his excellent and patient advising.

I also owe much to Miklós Abért, David Gabai, Márton Hablicsek, András Juhász, Sam Lewallen, Peter Ozsváth, Sucharit Sarkar, Cotton Seed, András Stipsicz, Vera Vértesi, Yang (Chris) Xiu, and Bohua Zhan for many helpful discussions at various points throughout my study and research.

Contents

Abstract iii

Acknowledgements iv

1 Introduction **1**

2 Brief overview of Heegaard Floer Homology **3**

2.1 Heegaard Floer homology 3

2.2 Heegaard Floer Knot Homology 7

2.2.1 The "Hat Version" $\widehat{HFK}$ 8

2.2.2 Algebraic refinements: HFK^- and HFK^∞ 9

2.3 Multi-pointed Heegaard diagrams 10

3 Heegaard Floer Homology and (1,1)-knots **12**

3.1 (1,1)-knots 12

3.2 Some earlier results on (1,1)-knots 13

3.3 Classification of (1,1)-knots up to 12 crossings 15

3.4 Genus one doubly pointed Heegaard diagrams 16

3.4.1 Minimal state and symmetry 17

3.4.2 Fundamental groups of $(1,1)$-knots 24

3.5 Knot Floer homology for (1,1)-knots 29

3.6 (1,1)-knots with trivial Alexander polynomial 33

3.7 Computational Tools and Proof of Theorem 3.3.1 35

3.7.1 Listing all candidate $(1,1)$-diagrams 36
3.7.2 Excluding $(1,1)$-diagrams that do not represent small knots 36
3.7.3 Identifying small knots represented by the remaining $(1,1)$-diagrams . 38

4 A new class of multi-pointed knot Heegaard diagrams 41

4.1 Perfect $(0,k)$-diagrams 42
4.2 Parallelizing $(0,k)$-diagrams 44
4.3 Constructing perfect $(0,k)$-diagrams 49
4.4 Geometry of perfect $(0,k)$-diagrams 51

Chapter 1

Introduction

Heegaard Floer homology is a recently invented technique in low-dimensional topology, introduced in 2001 by Ozsváth and Szabó [29]. In its original form, Heegaard Floer homology assigns graded modules to oriented closed 3-manifolds, giving a homeomorphism invariant. It essentially extracts the information captured by Seiberg–Witten invariants from a more elementary construction [18]. In this work, we are focusing more on the knot versions of Heegaard Floer homology, which assign algebraic invariants to knots and links.

$(1,1)$-knots are 1-bridge knots on the torus: knots in S^3 that may be cut by a standard torus in S^3 into two trivial arcs (one each in the resulting solid tori). The work of Morimoto–Sakuma–Yokota [22] and Klimenko–Sakuma [16] classified $(1,1)$-knots of up to 10 crossings, as well as $(1,1)$-knots that are also Montesinos knots (knots that support a particular tangle decomposition, see Section 3.2 for details), using results about the symmetry group of such knots.

By using Heegaard Floer invariants and observing symmetry properties of Heegaard diagrams for $(1,1)$-knots (Theorem 3.4.6), we provide a complete classification of $(1,1)$-knots up to 12 crossings. We also show a property of the Heegaard Floer homology of $(1,1)$-knots (Theorem 3.4.9), giving an integer-valued invariant. We conjecture that this property may be true for all knots in S^3, giving a concordance invariant that is independent

of some commonly used concordance invariants. We define and study subclass of $(1,1)$-knots for which the classical Alexander polynomial determines the knot's genus and whether the knot is fibered (Corollary 3.5.8).

In addition, we define a class of multi-pointed Heegaard diagrams for classical links (links in S^3), which we call *perfect* $(0,k)$*-diagrams*, that generalizes the well-known *grid diagrams*. Just like grid diagrams, perfect diagrams may be used to compute all variants of link Heegaard Floer homology combinatorially. We establish some results regarding the existence (Theorems 4.2.5 and 4.2.6) and structure (Theorem 4.4.1) of perfect $(0,k)$-diagrams.

In Chapter 2, we give a brief introduction to Heegaard Floer homology. For a more complete introduction, see [31].

In Chapter 3, we review some past results concerning $(1,1)$-knots as well as our own contributions, and use the power of Heegaard Floer Knot homology to classify certain $(1,1)$-knots.

In Chapter 4, we discuss perfect $(0,k)$-diagrams, a new class of multi-pointed Heegaard diagrams for links in S^3 (a generalization to the classical grid diagrams), and their use in Heegaard Floer homology.

Chapter 2

Brief overview of Heegaard Floer Homology

2.1 Heegaard Floer homology

Heegaard Floer homology is based on Lagrangian Floer homology (a tool from symplectic geometry), and it is defined through a Heegaard diagram of a closed oriented 3-manifold. Several interesting constructions follow from Heegaard Floer homology. It is functorial, in the sense that it assigns module maps to cobordisms of 3-manifolds; this can be used to define a smooth 4-manifold invariant. If a contact structure is given on the 3-manifold, one may obtain a contact invariant [30]. Most interestingly for us, Heegaard Floer homology can be adapted to get invariants for null-homologous knots and links in 3-manifolds [28] (often called Knot Floer homology).

These Knot Floer invariants can be viewed as an extension and generalization of the classical Alexander polynomial, while greatly surpassing its geometric descriptive power. For example, the Alexander polynomial yields a lower bound for the Seifert genus (3-ball genus) of a knot in S^3; Knot Floer homology determines the Seifert genus precisely [27]. It also detects whether such a knot is fibered [23]. The Ozsváth–Szabó τ-invariant, a closely

related concordance invariant for knots in S^3, provides a lower bound for the 4-ball genus and the unknotting number [26]; among other results, it yields an especially appealing proof for Kronheimer–Mrowka's theorem about the unknotting number of torus knots [17] (also known as the Milnor conjecture).

Now we give a very brief overview of the construction of Heegaard Floer homology.

A Heegaard decomposition means cutting the manifold Y^3 into two handlebodies along an oriented surface Σ of genus g; every oriented closed 3-manifold supports Heegaard decompositions. A Heegaard diagram comprises Σ and two sets of g pairwise disjoint, transverse, and homologically independent simple closed curves (i.e. embedded S^1's): $\alpha_1, \ldots, \alpha_g$ and $\beta_1, \ldots, \beta_g$, that bound discs in the two handlebodies respectively. Alternatively, in the language of Morse theory, if $f : Y \to \mathbb{R}$ is a self-indexing Morse function with a unique local minimum and maximum, we can take $\Sigma = f^{-1}\left(\frac{3}{2}\right)$, and the curves α_i and β_i are the circles where the ascending manifolds from critical points of index 1 and the descending manifolds from critical point of index 2 intersect Σ, respectively. The triplet $(\Sigma, \boldsymbol{\alpha}, \boldsymbol{\beta})$ determines Y^3 uniquely up to homeomorphism.

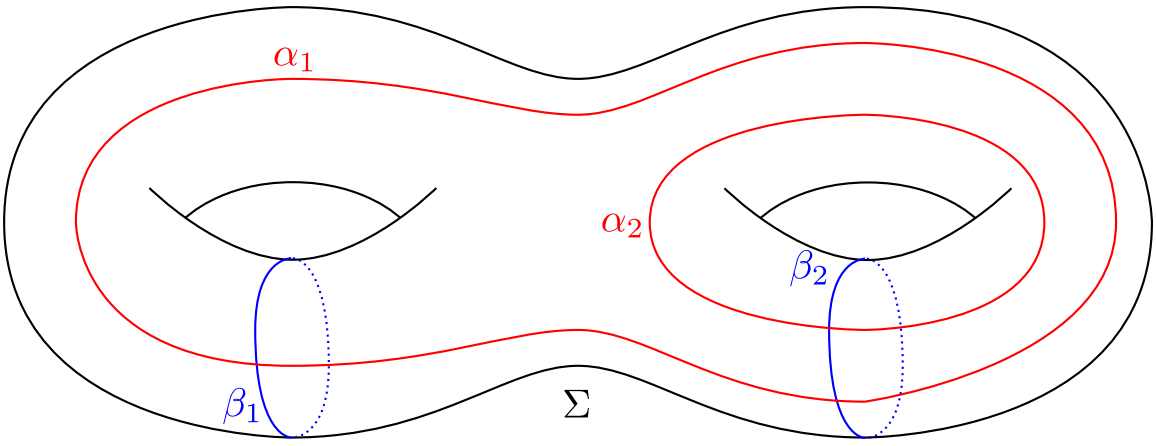

Figure 2.1: A Heegaard diagram (representing S^3)

By choosing a holomorphic structure on Σ (making it a 1-dimensional complex curve), one gets a holomorphic structure on $Sym^g(\Sigma)$, the g'th symmetric power of Σ (that is, the space of unordered g-tuples of points on Σ). Then, $Sym^g(\Sigma)$ is given a symplectic

structure compatible with this holomorphic structure, and we consider the submanifolds $\mathbb{T}_\alpha = \alpha_1 \times \cdots \times \alpha_g$ and $\mathbb{T}_\beta = \beta_1 \times \cdots \times \beta_g$. These manifolds of real dimension g are Lagrangian submanifolds in $Sym^g(\Sigma)$ (more specifically, they are totally real tori), and we consider their Lagrangian Floer homology $HF(\mathbb{T}_\alpha, \mathbb{T}_\beta)$ with some modifications.

The chain complex for this homology, $\widehat{CF}(Y^3)$ is generated by the intersection points $\mathbb{T}_\alpha \cap \mathbb{T}_\beta$ over the field $\mathbb{F}_2 = \mathbb{Z}/2\mathbb{Z}$.[1] In other words, the generators are all g-tuples $\boldsymbol{x} = (x_1, \ldots, x_g)$, such that $x_i \in \alpha_i \cap \beta_{\sigma(i)}$ for some permutation σ in the symmetric group on the set $\{1, 2, \ldots, g\}$.

The differential map $\widehat{\partial}$ is defined as follows. To compute the coefficient of generator $\boldsymbol{y}$ in $\widehat{\partial}(\boldsymbol{x})$, we fix a generic almost complex structure on $Sym^g(\Sigma)$ compatible with its symplectic structure, and count pseudo-holomorphic disks ϕ from $\boldsymbol{x}$ to $\boldsymbol{y}$. A pseudo-holomorphic disk from $\boldsymbol{x}$ to $\boldsymbol{y}$ is a continuous map ϕ from the closed unit disk in the complex plane $D \subset \mathbb{C}$ to $Sym^g(\Sigma)$, satisfying the following conditions:

- ϕ is differentiable, and compatible with the pseudo-holomorphic structure in the interior of D;
- $\phi(-i) = \boldsymbol{x}$ and $\phi(i) = \boldsymbol{y}$;
- If $u \in \partial D$ and $Re(u) > 0$, then $\phi(u) \in \mathbb{T}_\alpha$; if $u \in \partial D$ and $Re(u) < 0$, then $\phi(u) \in \mathbb{T}_\beta$. (The edges of the disk follow the two tori respectively.)

Furthermore, we require that ϕ have Maslov index 1. This means that, in a certain technical sense, ϕ has 0 real degrees of freedom (apart from the trivial re-parametrizations of the unit disk). The modulo 2 number of such pseudo-holomorphic disks is the coefficient of $\boldsymbol{y}$ in $\widehat{\partial}(\boldsymbol{x})$. Finally, to get a non-trivial invariant, one needs to puncture Σ at a *basepoint* z (disjoint from the α and β curves), which effectively forbids pseudo-holomorphic discs to pass through $z \times Sym^{g-1}(\Sigma)$.

[1] It is also possible to work over $\mathbb{Z}$ with a suitable sign convention for the differential map.

In a formula, the differential map $\widehat{\partial}$ may be given as

$$\widehat{\partial}x = \sum_{y \in \mathbb{T}_\alpha \cap \mathbb{T}_\beta} \sum_{\substack{\phi \in \pi_2(x,y) \\ \mu(\phi)=1 \\ n_z(\phi)=0}} y$$

for each generator $x \in \mathbb{T}_\alpha \cap \mathbb{T}_\beta$.

Ozsváth and Szabó proved that if certain technical conditions are satisfied, then $\widehat{\partial}$ described above is indeed a differential; furthermore, the resulting homology group $\widehat{HF}(Y^3) = HF_{Sym^g(\Sigma \setminus \{z\})}(\mathbb{T}_\alpha, \mathbb{T}_\beta)$ depends only on Y^3, and not on the various choices made during the construction.

One may obtain finer invariants by allowing ϕ to pass over the base point (i.e. intersect $z \times Sym^{g-1}(\Sigma)$), recording the number of such intersections by multiplying by an independent variable U. The homology $HF^-(Y^3)$ comes from the chain complex $(CF^-(Y^3), \partial^-)$, where $CF^-(Y^3) = \mathbb{F}[U]\langle \mathbb{T}_\alpha \cap \mathbb{T}_\beta \rangle$, i.e. the module generated by the same formal generators over the polynomial ring $\mathbb{F}[U]$. One may also allow negative powers of U, leading to the homology $HF^\infty(Y^3)$, coming from $(CF^\infty(Y^3), \partial^\infty)$, where $CF^\infty(Y^3) = \mathbb{F}[U, U^{-1}]\langle \mathbb{T}_\alpha \cap \mathbb{T}_\beta \rangle$, using the ring of Laurent polynomials $\mathbb{F}[U, U^{-1}]$. In CF^∞, multiplication by U (or U^{-1}) gives an automorphism, which is inherited by HF^∞.

In both cases, the differential map is described as

$$\partial^\infty x = \partial^- x = \sum_{y} \sum_{\substack{\phi \in \pi_2(x,y) \\ \mu(\phi)=1}} U^{n_z(\phi)} \cdot y,$$

where $n_z(\phi)$ is the number of intersections (with multiplicity) between ϕ and $z \times Sym^{g-1}(\Sigma)$. (Since both of these are pseudoholomorphic curves, all of the intersections must be positively oriented, so there is no difference between algebraic and geometric intersection numbers.)

Finally, one may define the complex $(CF^+(Y^3), \partial^+)$ as the quotient complex $(CF^\infty(Y^3), \partial^\infty)/(CF^-(Y^3), \partial^-)$. The short exact sequence

$$0 \to CF^-(Y^3) \to CF^\infty(Y^3) \to CF^+(Y^3) \to 0$$

gives rise to an exact triangle

$$HF^-(Y^3) \to HF^\infty(Y^3) \to HF^+(Y^3) \to HF^-(Y^3).$$

2.2 Heegaard Floer Knot Homology

Heegaard Floer Knot Homology (often shortened to Knot Floer homology) is a type of knot invariants that were defined by Ozsváth and Szabó [28], and independently by Rasmussen [33].

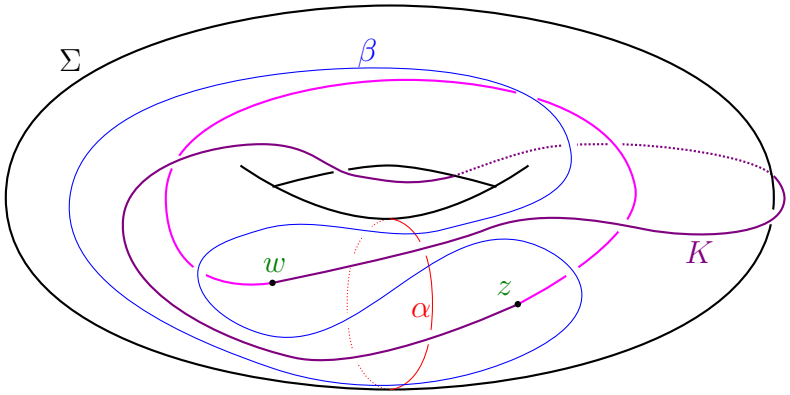

Figure 2.2: Doubly pointed Heegaard Diagram representing a trefoil

A knot K in an oriented closed 3-manifold Y can be represented by a doubly-pointed Heegaard diagram: $(\Sigma, \boldsymbol{\alpha}, \boldsymbol{\beta}, w, z)$, where $(\Sigma, \boldsymbol{\alpha}, \boldsymbol{\beta})$ is a Heegaard diagram for Y, and w, z are two base-points distinct from each other and the α and β curves. The knot may be recovered by connecting w and z in the handlebodies on each side of Σ.

2.2.1 The "Hat Version" $\widehat{HFK}$

By only counting pseudo-holomorphic disks that pass through neither w nor z, one may obtain the simplest Knot Floer homology invariant

$$\widehat{HFK}(Y,K) = HF_{Sym^g(\Sigma\setminus\{w,z\})}\left(\mathbb{T}_\alpha, \mathbb{T}_\beta\right).$$

As with the manifold case, this definition can be refined to obtain more powerful invariants.

We will be most interested in the case of classical knots, when $Y = S^3$. In this case, the chain complex $\left(\widehat{CFK}(S^3,K), \widehat{\partial}\right)$ supports two different $\mathbb{Z}$-gradings: the homological (or Maslov) grading that the boundary map $\widehat{\partial}$ decreases by 1, and the Alexander grading, which $\widehat{\partial}$ leaves invariant.

Definition 2.2.1. *If $u \in \Sigma \setminus \alpha_1 \setminus \cdots \setminus \alpha_g \setminus \beta_1 \setminus \cdots \setminus \beta_g$, $n_u(\phi)$ denotes the number of times ϕ "passes over" u, i.e. the algebraic intersection number $\#\phi^{-1}\left(\{u\} \times Sym^{g-1}(\Sigma)\right)$.*

Definition 2.2.2. *The* shadow *(also called* domain*) of a pseudo-holomorphic ϕ describes how many times ϕ passes over each region of Σ. If $D_1, \ldots, D_m$ are the connected components of $u \in \Sigma \setminus \alpha_1 \setminus \cdots \setminus \alpha_g \setminus \beta_1 \setminus \cdots \setminus \beta_g$, then the shadow of ϕ is the formal linear combination*

$$\mathcal{D}(\phi) = \sum_{i=1}^{m} n_{z_i}(\phi) D_i,$$

where $z_i \in D_i$.

If ϕ is a pseudoholomorphic disk of Maslov index 1 from x to y, then the gradings of x and y are related as follows:

$$A(x) - A(y) = n_z(\phi) - n_w(\phi);$$

$$M(x) - M(y) = 1 - 2n_w(\phi).$$

The homology $\widehat{HFK}(S^3, K)$ inherits these gradings:

$$\widehat{HFK}(S^3, K) = \bigoplus_{m,a \in \mathbb{Z}} \widehat{HFK}_m(S^3, K, a).$$

This bigraded group-valued invariant is stronger than the classical Alexander polynomial, and contains much information about the knot's geometry. Some of this information is summarized by the Poincaré polynomial

$$HF_K(q, t) = \sum_{m,a \in \mathbb{Z}} q^m \cdot t^a \cdot \mathrm{rk}\, \widehat{HFK}_m(S^3, K, a),$$

a Laurent polynomial in two variables with non-negative integer coefficients. The Alexander polynomial $\Delta_K(t)$ is just the Euler characteristic of $\widehat{HFK}$ in each Alexander grading: $\Delta_K(t) = HF_K(-1, t)$.

The (symmetrized) Alexander polynomial gives a lower bound for the genus of a knot: $\deg \Delta_K \leq g(K)$, where $\deg \Delta_K$ is the maximal $a \in \mathbb{Z}$ for which the coefficient of t^a in $\Delta_K(t)$ is nonzero. Knot Floer homology determines the genus exactly [27]: $\deg_a HF_K = g(K)$, where $\deg_a HF_K$ is the maximal $a \in \mathbb{Z}$ such that the coefficient of t^a in $HF_K(1, t)$ is nonzero.

The Alexander polynomial gives an obstruction to a knot being Seifert fibered: if K is fibered, then the leading coefficient of Δ_K (that belonging to $t^{\deg \Delta_K}$) is ± 1. Knot Floer homology gives an exact criterion for whether the knot is fibered ([23]; see also [10], [14]): K is fibered if and only if the leading coefficient of $HF_K(1, t)$ is 1.

2.2.2 Algebraic refinements: HFK^- and HFK^∞

The chain complex $\widehat{CFK}(S^3, K)$ is generated over the field $\mathbb{F} = \mathbb{Z}_2$. One may obtain finer invariants by considering modules over the ring of polynomials $\mathbb{F}[U]$ or Laurent polynomials $\mathbb{F}[U, U^{-1}]$:

$$CFK^-(S^3, K) = \mathbb{F}[U]\langle \mathbb{T}_\alpha \cap \mathbb{T}_\beta \rangle$$

$$CFK^\infty(S^3,K) = \mathbb{F}[U,U^{-1}]\langle \mathbb{T}_\alpha \cap \mathbb{T}_\beta\rangle$$

The boundary maps are adjusted to allow passing through z; the symbol U keeps track of the number of times this happens:

$$\partial^\infty x = \partial^- x = \sum_y \sum_{\substack{\phi\in\pi_2(x,y)\\ \mu(\phi)=1\\ n_w(\phi)=0}} U^{n_z(\phi)}\cdot y$$

Alternatively, one may use the symmetry between basepoints w and z (allowing holomorphic disks to pass through w but not z) to get $\widehat{HFK}$ for the same knot. As shown in [28], this yields a spectral sequence starting at Knot Floer homology and converging to $\mathbb{F}$, which in turn is used for the original definition of the integer-valued concordance invariant, the Ozsváth–Szabó invariant τ.

2.3 Multi-pointed Heegaard diagrams

Up to now, we have only considered classical Heegaard diagrams, where the Heegaard decomposition $Y = U_0 \cup_\Sigma U_1$ is described by g-tuples of pairwise distinct, homologically independent curves $\boldsymbol{\alpha}$ and $\boldsymbol{\beta}$ on the surface Σ of genus g. However, one may use homologically redundant curves at the price of introducing extra basepoints. In the Morse theory view, we now allow Morse functions with k local minima and maxima each.

A k-pointed Heegaard diagram for Y features $(g+k-1)$-tuples of pairwise distinct curves $\boldsymbol{\alpha}$ and $\boldsymbol{\beta}$, such that $H_1(\Sigma) = \langle\boldsymbol{\alpha}\rangle \oplus H_1(U_0) = \langle\boldsymbol{\beta}\rangle \oplus H_1(U_1)$, and there are k basepoints $z_1,\dots,z_k$, such that each component of $\Sigma \setminus (\alpha_1 \cup \dots \cup \alpha_{g+k-1})$ contains exactly one z_i (and respectively for the β-complement components). The definition of $\widehat{HF}(Y)$ can be generalized to allow multi-pointed Heegaard diagrams.

Multi-pointed diagrams can be extended to allow knots and links, by choosing $2\cdot k$ base points $z_1,\dots,z_k$ and $w_1,\dots,w_k$. The link is easiest to reconstruct from the Morse theory

view; one takes the union of complete flow-lines from minima to maxima through the w_i's, and from maxima to minima through the z_i's. This construction gives a piecewise smooth embedding of a knot or a link of up to k components (depending on the diagram) in Y. Knot Floer invariants (or in some cases, their stabilized versions) may be computed from such multi-pointed link diagrams.

Chapter 3

Heegaard Floer Homology and (1,1)-knots

3.1 (1,1)-knots

Following the terminology of Doll [7], we call a knot $K \subset S^3$ a (g, b)-*knot* (for nonnegative integers g, b) if it has a diagram on the genus g orientable surface Σ_g that is composed of b overpasses (bridges) and b underpasses in general position, so that the overpasses do not intersect, the underpasses do not intersect, and whenever an overpass meets an underpass, the overpass goes above.

More formally, let $\Sigma_g \subset S^3$ be a genus g oriented surface embedded into S^3 in the standard way (i.e. as the boundary of a handlebody). Consider its tubular neighborhood $U_g = (-\varepsilon, \varepsilon) \times \Sigma_g \subset S^3$, such that the projection p_2 to the second coordinate is a submersion.

A knot K in S^3 is said to be *b-bridge on the genus g surface*, or a (g, b)-knot in short, if it is isotopic to a knot $K' : S^1 \to U_g$ whose "vertical component" $p_1 \circ K' : S^1 \to (-\varepsilon, \varepsilon)$ is a Morse function with b local maxima (and minima). If $b = 0$, we require $p_1 \circ K'$ to be constant (i.e. K' maps to Σ_g). One may always eliminate one overpass at the expense of an extra handle; therefore, a (g, b) knot is also a $(g + 1, b - 1)$-knot.

We will consider $(1,1)$-knots, which are 1-bridge knots on the torus: knots that can be drawn on the standard torus with one "overpass" and one "underpass". Two simple examples for $(1,1)$-knots are $(0,2)$-knots (ordinary 2-bridge knots), and $(1,0)$-knots (torus knots).

It is known that $(1,1)$-knots are always prime [24] and reversible [22] (isotopic to a copy of themselves with the internal orientation of the knot reversed). The work of Morimoto–Sakuma–Yokota and Klimenko–Sakuma classified $(1,1)$-knots that are also Montesinos knots (Theorem 2.2 in [22] and Corollary C in [16]). Morimoto–Sakuma–Yokota also classified $(1,1)$-knots up to crossing number 10.

One of the main results of this chapter is Theorem 3.3.1, which extends this classification to knots of up to 12 crossings.

3.2 Some earlier results on (1,1)-knots

The Conway notation, introduced in [6], offers a valuable tool to understand the structure of knots, building them up from rational tangles. A Montesinos knot is one that can be obtained from a "sum" of rational tangles using Conway's "+" operation (also denoted by "," in some sources). In simpler terms, this means that the knot can be represented by a diagram of the form shown on Figure 3.1, where each circle represents a rational 2-tangle.

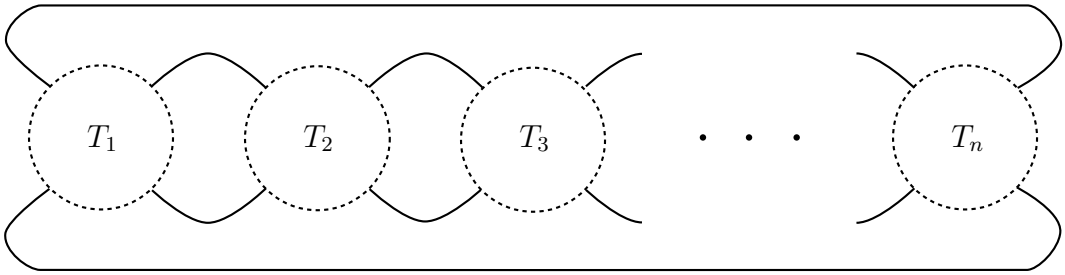

Figure 3.1: Structure of a Montesinos knot

The tunnel number $t(K)$ of a knot $K \subset S^3$ is defined to be the minimum number of tunnels one has to dig (i.e. removing a neighborhood of a properly embedded arc) in the

knot exterior such that the remainder is a handlebody. $t(K) = 0$ only if K is the unknot. It is easy to show that $\mathrm{rk}\left(\pi_1\left(S^3 \setminus K\right)\right) \leq t(K) + 1$; conjecturally, equality always holds.

In this chapter, we are mainly concerned with $(1,1)$-knots: 1-bridge knots on the torus. It is well-known that all $(1,1)$-knots are tunnel number 1 (e.g. [22]). (However, the converse is not true.)

In [22], Morimoto, Sakuma and Yokota proved the following statements about tunnel number one knots:

Theorem 3.2.1 (Morimoto, Sakuma and Yokota; Theorem 2.2 in [22]). *Let $K = M(b; (\alpha_1, \beta_1), \cdots (\alpha_r, \beta_r))$ be a Montesinos knot (not a link) with r branches. Suppose K has tunnel number one, then one of the following conditions holds up to cyclic permuiation of the indices:*

(1) $r = 2$.

(2) $r = 3$, $\alpha_1 = 2$, and $\alpha_2 \equiv \alpha_3 \equiv 1(\mod 2)$.

(3) $r = 3$, $\beta_2/\alpha_2 \equiv \beta_3/\alpha_3 \in \mathbf{Q}/\mathbf{Z}$, and $e(K) = \pm 1/(\alpha_1\alpha_2)$.

Conversely, if the condition (1), (2), or the following (3') holds, then K has tunnel number one:

(3') $r = 3$, $\beta_2/\alpha_2 \equiv \beta_3/\alpha_3 \equiv \pm 1/3 \in \mathbf{Q}/\mathbf{Z}$, and $e(K) = \pm 1/(3\alpha_1)$.

Theorem 3.2.2 (Morimoto, Sakuma and Yokota; Theorem 2.6 in [22]). *Let K be a prime knot with $\leqq 10$ crossings. Then $t(K) = 2$ if and only if K is equivalent to one the following knots; otherwise, $t(K) = 1$:*

8_n *with* $n \in [16, 18]$,

9_n *with* $n \in \{29\} \cup [32, 35] \cup [37, 41] \cup [46, 49]$,

10_n *with* $n \in [61, 69] \cup [74, 75] \cup [79, 123] \cup [140, 144] \cup [146, 160] \cup [163, 166]$.

In addition, they claim the following result:

Proposition 3.2.3 (Morimoto, Sakuma and Yokota; Remark 4.2 in [22]). *A Montesinos knot admits a $(1,1)$-decomposition if and only if it satisfies the condition (1), (2) or (3) of Theorem 2.2.*

Together with Corollary C in [16], this implies that for Montesinos knots, tunnel number one knots and (1,1)-knots are in fact the same.

3.3 Classification of (1,1)-knots up to 12 crossings

The above results imply a complete characterization of $(1,1)$-knots up to crossing number 10; worth noting is the fact that the only non-Montesinos $(1,1)$-knot in this set is the Perko "pair" $10_{161} = 10_{162}$, which may be represented by the Conway notation $[3 : -20 : -20]$. Using computations of Knot Floer homology as well as other knot invariants, we will extend this characterization up to crossing number 12 to yield further examples of non-Montesinos $(1,1)$-knots. We will prove the following

Theorem 3.3.1. *The complete list (up to mirror image) of non-Montesinos* $(1,1)$*-knots up to crossing number* 12 *is as follows:*

Name	Conway notation	Name	Conway notation	Name	Conway notation
10_{161}	$[3 : -20 : -20]$	$11n_{96}$	$[-2110 : 20 : 20]$	$11n_{111}$	$[-310 : 20 : 20]$
$11n_{135}$	$[22 : -20 : -20]$	$12n_{352}$	$[2110 : -210 : 20]$	$12n_{370}$	$[-210. - 21. - 20.20]$
$12n_{371}$	$[210. - 21. - 20.20]$	$12n_{374}$	$[2.2.2.20. - 21]$	$12n_{404}$	$[.3.20. - 21.20]$
$12n_{433}$	$[8 * 20. - 21 : .2]$	$12n_{446}$	$[2. - 210.2.210]$	$12n_{464}$	$[9 * 2. - 210]$
$12n_{483}$	$[10 * * - 2 - 1]$	$12n_{487}$	$[210. - 2. - 20.30]$	$12n_{488}$	$[-210. - 2. - 20.30]$
$12n_{500}$	$[. - 21.4.20]$	$12n_{501}$	$[. - 21.31.20]$	$12n_{502}$	$[.2.4. - 210]$
$12n_{503}$	$[.2.31. - 210]$	$12n_{552}$	$[2. - 2. - 20.2110]$	$12n_{579}$	$[-2.2. - 2.21.20]$
$12n_{591}$	$[30. - 21. - 20.20]$	$12n_{594}$	$[3. - 21. - 20.20]$	$12n_{624}$	$[8 * -210 : .2 : . - 20]$
$12n_{650}$	$[8 * -210.20. - 20]$	$12n_{749}$	$[-2.2. - 2.2.3]$	$12n_{851}$	$[311 : -20 : -20]$

(The Conway notations are taken from KnotInfo [5].)

We will return to the proof in Section 3.7 in more detail after discussing some basic properties of $(1,1)$-knots and how knot Floer homology applies to them. For now, we give a brief overview of the proof for Theorem 3.3.1.

To establish this result, we need to show two things:

- Represent the knots listed above as (1,1)-knots;
- Show that the knots missing from the list are not (1,1).

Knot Floer homology allows us to perform a brute force search among all suitable (1,1)-knots. Once a minimal (in the sense defined later) doubly pointed Heegaard diagram is given for a particular knot K, the diagram's complexity is bounded by $\mathrm{rk}\left(\widehat{HFK}(S^3, K)\right)$. We use Baldwin and Gillam's list [2] to compare the bigraded $\widehat{HFK}$ ranks between known knots of low crossing number, and (1,1)-knots.

Where the bigraded ranks match, we count homomorphisms $\pi_1(S^3 \backslash K) \to G$ into different finite groups G to filter false matches. When both the $\widehat{HFK}$ ranks and these invariants match, we construct an ordinary knot diagram (on S^2) for the (1,1)-knot. A purpose-made heuristic diagram-simplifying program shows that the number of crossings can indeed be reduced to 12 or below using Reidemeister moves. Once this is known, the other invariants uniquely identify which knot pertains to the (1,1)-presentation in question.

3.4 Genus one doubly pointed Heegaard diagrams

In this section, we analyze genus one doubly pointed Heegaard diagrams of S^3 (in the following: $(1,1)$-diagrams) to better understand the $(1,1)$-knots that they represent. Note that $g = 1$ means we are working on the two-dimensional torus $\Sigma = S^1 \times S^1$, and we only have a single α- and β-curve. Therefore, the slight abuse of notation $\alpha = \{\alpha_1\} = \{\alpha\}$ (and similarly for β) will not cause any confusion.

We recall some common Heegaard diagram terminology:

Definition 3.4.1. *A* polygon *in a Heegaard diagram ($2n$-gon: bigon, rectangle, hexagon, etc.) is a connected set $C \subset \Sigma$ such that $\partial C \subset \alpha \cup \beta$, C is homeomorphic to the closed disk D^2, and ∂C contains $2n$ intersection points $x \in \alpha \cap \beta$ (and n segments of α and β each).*

Definition 3.4.2. *A polygon is* empty *if it contains no base points.*

3.4.1 Minimal state and symmetry

All Heegaard diagrams $\mathcal{D}$ can be isotoped into a diagram $\mathcal{D}_0(\Sigma, \alpha, \beta, z, w)$ where α and β are transverse, and there are no empty bigons. Furthermore, the result is unique up to homeomorphism (Theorem 2.10 of [25] applies with minimal modifications). We will call such a diagram a *minimal diagram*. In this section, we will focus mainly on minimal $(1,1)$-diagrams.

Holomorphic discs are easier to find for genus 1 than in the general case:

Proposition 3.4.3 (Ozsváth–Szabó [28])**.** *If $\mathcal{D}$ is a Heegaard diagram over the torus (i.e. of genus $g = 1$), then all pseudoholomorphic disks are immersed bigons.*

Thus, it is particularly easy to compute the "hat version" of knot Floer homology for minimal $(1,1)$-diagrams:

Proposition 3.4.4 (Example in Ozsváth–Szabó [28], general case in Goda–Matsuda–Morifuji [11] and Doyle [8])**.** *If $\mathcal{D}$ is a minimal $(1,1)$-diagram, the differential map $\widehat{\partial} : \widehat{CFK} \to \widehat{CFK}$ is trivial, i.e. $\widehat{HFK} = \widehat{CFK}$.*

Corollary 3.4.5. *For a minimal $(1,1)$-diagram $\mathcal{D}$, the total rank of the hat version of knot Floer homology is equal to the number of intersection points $\alpha \cap \beta$; in other words, the more general inequality $\operatorname{rk} \widehat{HFK} \leq |\mathbb{T}_\alpha \cap \mathbb{T}_\beta|$ is sharp.*

We now add an observation about minimal $(1,1)$-diagrams. If $\mathcal{D}$ is a minimal $(1,1)$-diagram, it shows a nontrivial symmetry:

Theorem 3.4.6. *If $\mathcal{D}(\Sigma, \alpha, \beta, z, w)$ is a minimal $(1,1)$-diagram, then there is an orientation-preserving homeomorphism $\iota : \Sigma \to \Sigma$ such that*

- *ι is an involution, i.e. $\iota^2 = \mathrm{id}_\Sigma$;*
- *ι maps α to itself and β to itself, but reverses their respective orientations;*
- *$\iota(w) = z$ and $\iota(z) = w$;*

- *ι fixes exactly one intersection point $x_0 \in \alpha \cap \beta$.*

Proof. First, note that since $\mathcal{D}$ is a Heegaard diagram for S^3, the algebraic intersection number of the curves is known: $\#(\alpha \cap \beta) = \pm 1$. (With a suitable change of orientation of α, we can assume it is in fact 1.) This means that if the number of negative intersections of α and β is k, then the number of positive intersections is $k+1$. In any case, the total number is odd: $n = |\alpha \cap \beta| = 2k+1$.

α is subdivided by β into n arc segments. We call such an arc segment a *loop* if it represents $0 \in H_1(\Sigma, \beta)$ and a *bridge* otherwise. Since Σ and β are oriented, we can consistently define the left and right sides of β. Each loop returns to the same side of β, while each bridge connects different sides. Thus, if there are r loops going to the left of β, then there are r loops going to the right, and $2(k-r)+1$ bridges connecting the two sides.

As Rasmussen shows (Section 6.2 of [32]; note that we deviate from Rasmussen's notations), a minimal diagram features two sets of r parallel loops (enclosing w and z respectively), and one or two sets of parallel bridges. Here, *parallel* arcs mean non-intersecting sections of a tubular neighborhood of an arc. (See Figure 3.2 for an example.) Let us denote by s the number of bridges crossing "to the left" ($t = 2(k-r)+1-s$ bridges cross to the right; set $s = 0$ if all bridges are parallel).

Now, let us index the n intersection points of α and β by elements of the cyclic group $Z_n = \mathbb{Z}/n\mathbb{Z}$, according to their oriented order on β. Recall that n is odd. If x_i and x_j ($i,\ j \in Z_n$) are connected by a loop on the left side of β, let us define $c_l = \frac{i+j}{2} \in Z_n$. Since all such loops are parallel, c_l is independent of the loop we chose. (If there are no loops, i.e. $r = 0$, then all intersections have the same sign, so $n = 1$ follows; in this case, set $c_l = 0$.) Similarly, define c_r for loops to the right of β. Let $m = \frac{c_l + c_r}{2}$. Let $c = c_l - m = m - c_r \in Z_n$.

Without loss of generality, we can assume that $m = 0$ (re-label the intersections so that x_i goes to x_{i-m}). If this is the case, we can uniquely describe all arcs in terms of the numbers k, r, c and s:

- r loops connect x_{c-i} to x_{c+i} on the left side of β ($k - r < i \leq k$)

- r loops connect $x_{-(c-i)}$ to $x_{-(c+i)}$ on the right side of β $(k-r<i\leq k)$
- s bridges connect the left side of β at x_i and the right side of β at x_j where $c-k+r\leq i<c-k+r+s$, $-(c-k+r+s)<j\leq -(c-k+r)$, and $i-j=2(c-k+r)+s-1$
- t bridges connect the left side of β at x_i and the right side of β at x_j where $c+k-r-t<i\leq c+k-r$, $-(c+k-r)\leq j<-(c+k-r-t)$, and $i-j=2(c-k+r)-t+1$

Thus, we observe the following:

1. x_i and x_j are connected by a loop to the *left* of $\beta \iff$
   x_{-i} and x_{-j} are connected by a loop to the *right* of β
2. A bridge connects the left side of β at x_i and the right side of β at $x_j \iff$
   A bridge connects the right side of β at x_{-i} and the left side of β at x_{-j}

Let $\iota : \alpha\cap\beta \to \alpha\cap\beta$ be the map $\iota(x_i)=x_{-i}$. Thanks to the above, we can extend ι to be a homeomorphism on the curves: $\iota : \alpha\cup\beta\to\alpha\cup\beta$. Since the topology of polygons and their gluings is uniquely determined by their combinatorics, we can further extend this homeomorphism to $\iota:\Sigma\to\Sigma$. We immediately observe that ι preserves the orientation of Σ and reverses that of β; by inspecting it at x_0, we also see that it reverses the orientation of α as well.

Consider the smallest bigons containing the base points w and z respectively; they are enclosed by the loop between $\frac{c-1}{2}=c+k$ and $\frac{c+1}{2}=c-k$ (on the left of β), and its dual pair between $-c-k$ and $-c+k$ (on the right of β). (Without loss of generality, we assume that w is contained in the former bigon and z in the latter: if not, reverse the orientation of both α and β.) We can apply an isotopy in $\Sigma\setminus\alpha\setminus\beta$ to make sure that $\iota(w)=z$.

□

Corollary 3.4.7. *Let us consider the numbers $k\in\mathbb{Z}_{\geq 0}$, $r\in\mathbb{Z}\cap[0,k]$, $c\in Z_{2k+1}$ and $s\in\mathbb{Z}$. Since $0\leq s<2(k-r)+1$, we can represent it as $s\in Z_{2(k-r)+1}$; note that this removes the ambiguity of notation from the case $s=0$ (when all bridges are parallel).*

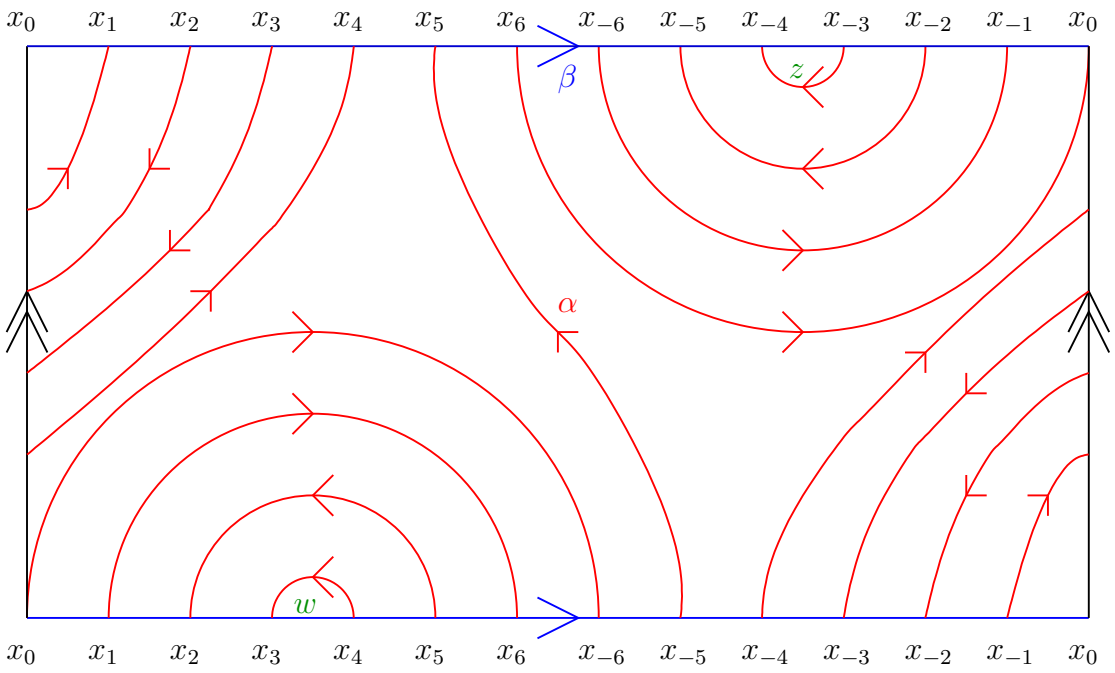

Figure 3.2: $\mathcal{D}_{(1,1)}(6,4,-3,-1)$, representing the "Perko pair" knot 10_{161} (cf. [11])

The above proof gives us a map

$$\{\text{minimal } (1,1)\text{-diagrams } \mathcal{D}\}/\{\text{orientation-preserving homeomorphisms of } \Sigma\}$$

$$\downarrow$$

$$\{(k,r,c,s) : k \in \mathbb{Z}_{\geq 0}, r \in \mathbb{Z} \cap [0,k], c \in Z_{2k+1}, s \in Z_{2(k-r)+1}\}$$

It is straightforward to define the inverse map

$$\mathcal{D}_{(1,1)} : \left\{(k,r,c,s) : k \in \mathbb{Z}_{\geq 0}, r \in \mathbb{Z} \cap [0,k], c \in Z_{2k+1}, s \in Z_{2(k-r)+1}\right\} \to (\Sigma, \alpha, \beta, w, z);$$

although the resulting diagram $(\Sigma, \alpha, \beta, w, z)$ will not be a Heegaard diagram for some values of (k,r,c,s): the α-arcs may fail to yield one connected α-curve. Even if we get a valid Heegaard diagram, it may represent a knot in a different lens space rather than S^3. Nevertheless, we will use the notation $\mathcal{D}_{(1,1)}(k,r,c,s)$ to denote this diagram, with the understanding that (k,r,c,s) are chosen such that the resulting diagram is a Heegaard diagram of some $K \subset S^3$.

$\mathcal{D}_{(1,1)}(k,r,c,s)$ is an improvement over previous parametrizations in two ways: the diagram determines the parametrization uniquely, and the mirror image of the underlying knot is represented by $\mathcal{D}_{(1,1)}(k,r,-c,-s)$.

Using the above, we get a new proof of the well-known fact:

Corollary 3.4.8. *All $(1,1)$-knots are reversible.*

Proof. If $(\Sigma,\alpha,\beta,w,z)$ is a doubly-pointed Heegaard diagram for our knot K, then $(\Sigma,\alpha,\beta,z,w)$ represents the reverse $r(K)$. However, $(\Sigma,\alpha,\beta,z,w) = (\Sigma,\iota(\alpha),\iota(\beta),\iota(w),\iota(z))$, which is homeomorphic (in the oriented sense) to the original diagram $(\Sigma,\alpha,\beta,w,z)$ for K. □

Let us introduce the notation

$$d_K(a,m) = \operatorname{rank}\left(\widehat{HFK}_a\left(S^3,K,m\right)\right).$$

Theorem 3.4.6 also yields a natural involution of $\widehat{HFK}(S^3,K)$ that induces the known symmetry relation $d_K(a,m) = d_K(-a,m-2a)$. in the case of (1,1)-knots. In fact, it gives slightly more:

Corollary 3.4.9. *For a (1,1)-knot K, there is a unique Maslov grading m such that the rank at Maslov grading m and Alexander grading zero, i.e. $d_K(0,m)$ is odd. This integer m is thus an invariant of K.*

Let us introduce a name for this property:

Definition 3.4.10. *A knot $K \subset S^3$ has the* unique odd property *(with respect to knot Floer homology) if there is a unique Maslov grading m such that the rank of $\widehat{HFK}(S^3,K)$ at Maslov grading m and Alexander grading zero, i.e. $d_K(0,m)$ is odd.*

Definition 3.4.11. *For a knot $K \in S^3$ let us denote by $\mu_0(K)$ the set of values $m \in Z$ such that $d_K(0,m)$ is odd.*

The set $\mu_0(K)$ may be regarded as a knot invariant. $|\mu_0(K)|$ is odd for each knot K, and is 1 if and only if K has the unique odd property. (In this case, with a slight abuse of notation, we will also write $\mu_0(K)$ for the unique element of this set.)

It might be interesting to see how common the unique odd property is. It does hold for a wide assortment of knots:

Proposition 3.4.12. *All knots in the following families have the unique odd property:*

- *(1,1)-knots*
- *Quasi-alternating knots [28]*
- *Whitehead doubles (as shown by Hedden [13])*
- *All knots up to 12 crossings (based on Baldwin–Gillam [2])*
- *Composite knots $K_1\#K_2$, provided it is true for both K_1 and K_2*

Proof. We only prove the case of composite knots $K_1\#K_2$, as the other families are straightforward to check based on the cited results.

Let us recall the symmetry relation $d_K(a,m) = d_K(-a, m-2a)$ and the Künneth-type formula [28]

$$\widehat{HFK}(S^3,K) = \widehat{HFK}(S^3,K_1) \otimes \widehat{HFK}(S^3,K_2).$$

Reordering the equations that we get for d_K from the tensor product, we have:

$$\begin{aligned} d_K(0,m) = \sum_{a=1}^{\infty}\sum_{j=-\infty}^{\infty} \Big(& d_{K_1}(a,j)\cdot d_{K_2}(-a,m-j) + \\ & d_{K_1}(-a,j-2a)\cdot d_{K_2}(a,2a+m-j)\Big) + \\ & \sum_{j=-\infty}^{\infty} d_{K_1}(0,j)\cdot d_{K_2}(0,m-j). \end{aligned}$$

Since in the first sum

$$d_{K_1}(a,j)\cdot d_{K_2}(-a,m-j) = d_{K_1}(-a,j-2a)\cdot d_{K_2}(a,2a+m-j)$$

by the symmetry relation, the first sum is divisible by 2.

This means that the parity is determined by the second sum (a discrete convolution). Since K_1 and K_2 have the unique odd property, the convolution is applied to Kronecker δ functions $d_{K_i}(0,j) = \delta(\mu_0(K_i), j)$ (mod 2), so the result is $d_{K_1\#K_2}(0,j) = \delta(\mu_0(K_1) + \mu_0(K_2), j)$, i.e. $K_1\#K_2$ has the unique odd property and $\mu_0(K_1\#K_2) = \mu_0(K_1)+\mu_0(K_2)$. □

We mention the following optimistic conjectures:

Conjecture 3.4.13. *Every knot $K \subset S^3$ has the unique odd property.*

(A less ambitious version of Conjecture 3.4.13 would be to restrict it to reversible knots.) Based on Proposition 3.4.12, it would be enough to show this conjecture for prime knots.

Remark 3.4.14. *If we could show that $\mu_0(K') = \{0\}$ for each smoothly slice knot K', that would prove Conjecture 3.4.13. This is because μ_0 respects the mirror image operation: $\mu_0(m(K)) = -\mu_0(K)$, and $K' = K\#m(K)$ is smoothly slice.*

If Conjecture 3.4.13 holds, we make an even more optimistic conjecture based on the proof of Proposition 3.4.12:

Conjecture 3.4.15. *μ_0 is an integer-valued concordance invariant.*

Remark 3.4.16. *While μ_0 is a multiple of well-known concordance invariants such as the signature, the Ozsváth–Szabó τ invariant, and Rasmussen's s invariant for alternating knots, this is no longer true for all knots with the unique odd property. For the torus knot $T(3,4)$ for example, $\mu_0(T(3,4)) = 2$, while the linear rescaling of the aforementioned invariants would give* 3.

3.4.2 Fundamental groups of $(1,1)$-knots

We now recall classical results about the presentation of the fundamental group of a $(1,1)$-knot, given its $(1,1)$-diagram, and give explicit formulas for the presentation. This allows us to construct additional invariants to aid classification.

In addition to presenting $\pi_1(S^3 \setminus \mathrm{nd}\, K)$ as an abstract group, we use the standard framing of the knot to express a (meridian, longitude) pair – sometimes called a *peripherial system*, see e.g. [9]. This allows for finer invariants than the isomorphism type of the fundamental group alone.

Lemma 3.4.17. *Let $\mathcal{D}(\Sigma, \alpha, \beta, z, w)$ denote an oriented $(1,1)$-diagram representing an oriented knot $K \subset S^3$. Let $\bar{\mu} : [0,1] \to \Sigma \setminus \beta$ be a smooth simple curve connecting $w = \bar{\mu}(0)$ to $z = \bar{\mu}(1)$ that is transverse to α ($\bar{\mu} \pitchfork \alpha$). Compose a word w in the free group $F_2 = \langle b, m | \emptyset \rangle$ by following along α and noting its intersecion points with β and $\bar{\mu}$ respectively (see Figure 3.3):*

Parametrize α as $\alpha : S^1 = [0,1]/(0 \sim 1) \to \Sigma$. Let $\{t_1, t_2, \ldots, t_k\} = \{t | \alpha(t) \in \beta \cup \bar{\mu}\}$ such that $0 \leq t_1 < t_2 < \cdots < t_k < 1$. Let $w = g_1^{\varepsilon_1} g_2^{\varepsilon_2} \ldots g_k^{\varepsilon_k}$, where

- *$g_i = b$ if $\alpha(t_i) \in \beta$ and $g_i = m$ if $\alpha(t_i) \in \bar{\mu}$*
- *ε_i is the sign of the intersection at $\alpha(t_i)$*

Then, $\pi_1(S^3 \setminus \mathrm{nd}(K)) = \langle b, m | w = 1 \rangle$ with some elements $b, m \in \pi_1(S^3 \setminus \mathrm{nd}(K))$, where m is an oriented meridian of the knot K.

Proof. Consider the handlebody decomposition $S^3 = U_0 \cup_\Sigma U_1$, where β bounds a disk in U_0. Drill a tubular neighborhood $\mathrm{nd}(K)$ out of U_0, to obtain a 3-manifold with boundary $Y = U_0 \setminus nd(K)$.

In fact, since $K \cap U_0$ is a trivial arc in U_0, Y is a handlebody. β still bounds a disk $D^2(\beta)$ in Y. Let $\mu : S^1 \to \partial Y$ be an embedded oriented circle that closes the ends of curve

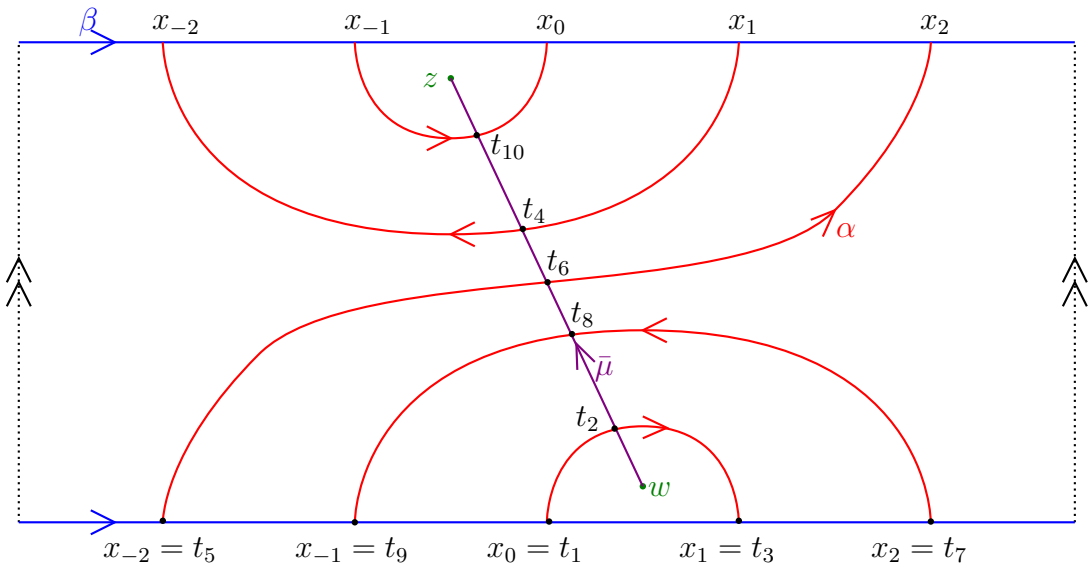

Figure 3.3: Constructing the word w for $\mathcal{D}_{(1,1)}(2, 2, -2, 0)$ (the figure 8 knot).

$\bar{\mu}$ around the tunnel, i.e. such that $\operatorname{Im}\mu \cap \Sigma = \operatorname{Im}\bar{\mu} \cap \Sigma$. Observe that μ also bounds a disk $D^2(\mu)$ in Y, and the homology classes $[\beta], [\mu] \in H_1(\partial Y)$ are independent. (See Figure 3.4.)

Pick a base point $x_0 \in \Sigma \cap \partial Y$ for π_1 such that $x_0 \notin \beta \cup \mu$. There is a deformation retraction of Y ending in a "figure eight": $r : Y \to S^1_b \vee_{x_0} S^1_m$, such that $r(D(\beta)) = x_b \in S^1_b \setminus \{x_0\}$ and $r(D(\mu)) = x_m \in S^1_m \setminus \{x_0\}$.

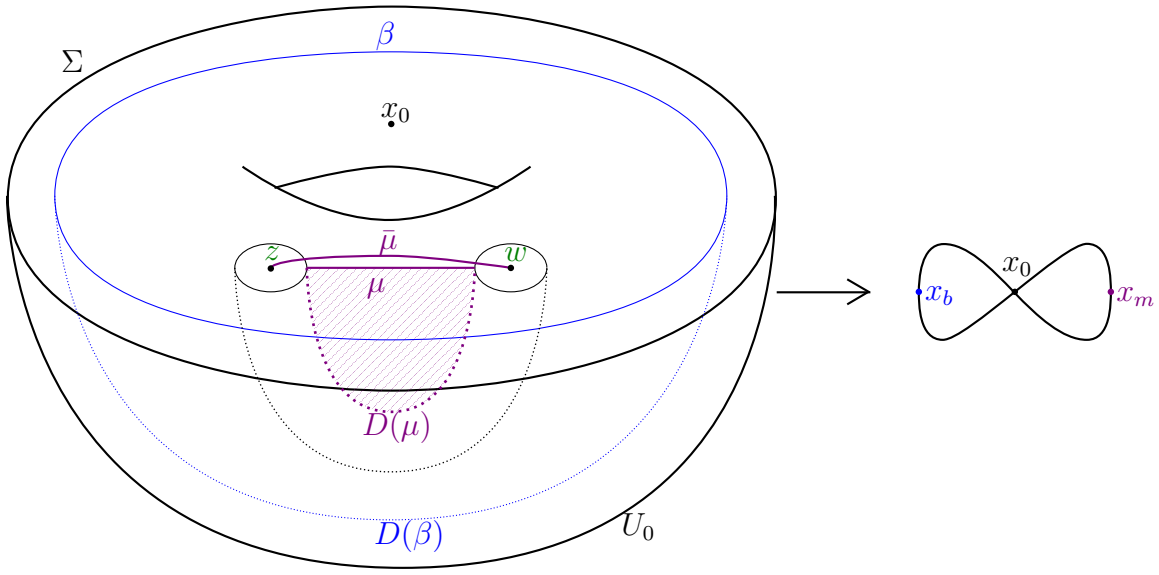

Figure 3.4: Curves and disks in manifold Y

Now, glue a disk (add a 2-handle) $D(\alpha)$ to Y along α, resulting in the 3-manifold with boundary N. On the one hand, observe that N is homeomorphic to the knot exterior $S^3 \setminus \mathrm{nd}(K)$. On the other hand, the fundamental group of N is $\pi_1(N) = \pi_1(Y)/[\alpha]_{\pi_1(Y)}$. Using the deformation retraction r shown above, we can conclude that $\pi_1(Y) = \langle b, m\rangle$ (where b and m are arbitrary liftings of S^1_b and S^1_m, respectively, at r), and $[\alpha]_{\pi_1(Y)} = w$. Finally, due to the construction of $D(\mu)$, any choice of m is a meridian of K. □

Remark 3.4.18. *Consider the Abelianization homomorphism $A : \pi_1(S^3 \setminus \mathrm{nd}(K)) \to H_1(S^3 \setminus \mathrm{nd}(K))$. The equation $w = g_1^{\varepsilon_1} g_2^{\varepsilon_2} \dots g_k^{\varepsilon_k} = 1$ maps to*

$$A(w) = \varepsilon_1 \cdot A(g_1) + \varepsilon_2 \cdot A(g_2) + \dots + \varepsilon_k \cdot A(g_k) = c_b A(b) + c_m A(m) = 0,$$

where c_b and c_m are the sum of the respective coefficients. As $\#(\beta \cap \alpha) = -\#(\alpha \cap \beta) = -1$, we conclude that $c_b = -1$; hence, $A(b) = c_m A(m)$.

In fact, we already knew that $A(b)$ has to be a multiple of $A(m)$, since the latter generates $H_1(S^3 \setminus \mathrm{nd}(K)) \equiv Z$. The computation above yields a formula for the factor c_m.

Lemma 3.4.19. *Using the notations in Lemma 3.4.2, let $\bar{\lambda} : [0,1] \to \Sigma \setminus \alpha$ be a smooth simple curve connecting $w = \bar{\lambda}(0)$ to $z = \bar{\lambda}(1)$ that is transverse to β and $\bar{\mu}$. Construct the word $l \in \langle b, m\rangle$ in a similar fashion to w, but using $\bar{\lambda}$ instead of α (see Figure 3.5):*

Let $\{t_1, t_2, \dots, t_k\} = \{0 < t < 1 | \bar{\lambda}(t) \in \beta \cup \bar{\mu}\}$ such that $0 < t_1 < t_2 < \dots < t_k < 1$. Let $l = g_1^{\varepsilon_1} g_2^{\varepsilon_2} \dots g_k^{\varepsilon_k}$, where

- *$g_i = b$ if $\lambda(t_i) \in \beta$ and $g_i = m$ if $\bar{\lambda}(t_i) \in \bar{\mu}$*
- *ε_i is the sign of the intersection at $\bar{\lambda}(t_i)$*

Then, there is an integer $j \in \mathbb{Z}$ such that $l_0 = l \cdot m^j \in \pi_1(S^3 \setminus \mathrm{nd}(K))$ is a longitude of K.

Proof. Consider the torus $T = \partial \mathrm{nd}(K) = \partial N$ around the knot. Without loss of generality, we may assume that the base point for π_1 (i.e. x_0) lies on T.

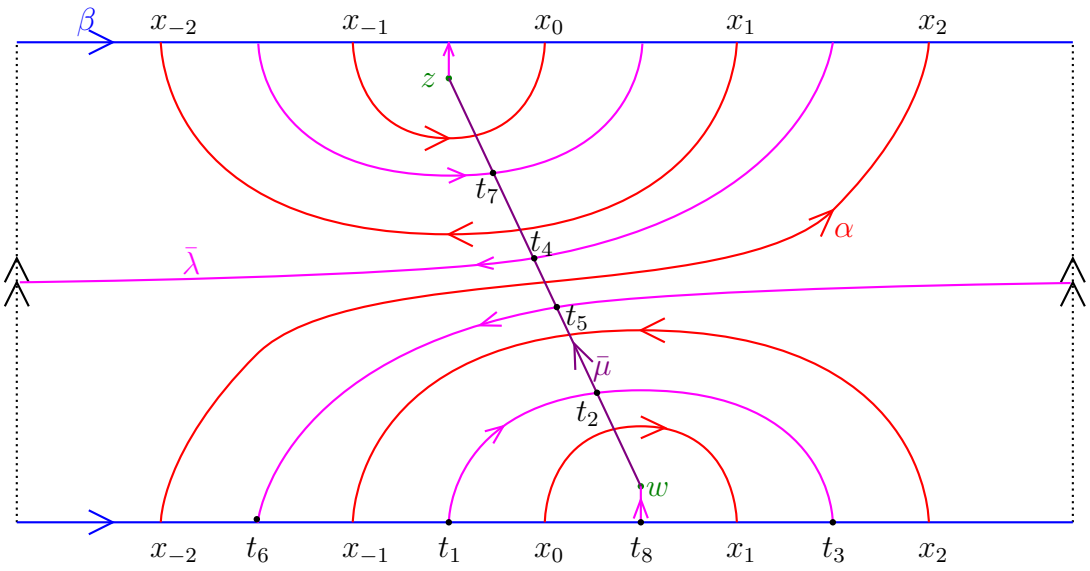

Figure 3.5: Constructing the word l for $\mathcal{D}_{(1,1)}(2,2,-2,0)$

We have a map from T to the knot: projection $p : T \hookrightarrow \overline{\mathrm{nd}(K)} \twoheadrightarrow K$, and to the knot complement: $\iota : T \hookrightarrow S^3 \setminus \mathrm{nd}(K)$. If we find a loop $l' \in \pi_1(T)$ such that $p_*(l') = [K] \in \pi_1(K) = H_1(K)$ is the fundamental class of K, then l' runs parallel to K. Then, just subtract the meridian component of l' to eliminate any nontrivial linking with the knot: $l'_0 = \iota_*(l' \cdot m^{-\mathrm{lk}(l',K)})$ is a longitude.

Let $\lambda : S^1 \hookrightarrow T \cap Y$ be a smooth simple closed curve such that extends $\bar{\lambda}$: $\mathrm{Im}\,\lambda \cap T = \mathrm{Im}\,\bar{\lambda} \cap T$, preserving the orientation of $\bar{\lambda}$ as well (see Figure 3.6). Observe that λ passes through the tunnel $U_0 \setminus nd(K)$ exactly once; thus, $\#(\lambda \cap D^2(\mu)) = 1$, so in fact $l' = [\lambda]_{\pi_1(T)}$ runs parallel to K.

Further, since $\mathrm{Im}\,\lambda \subset Y \setminus \alpha$ (away from $D^2(\alpha)$), we can use the deformation retraction r to project it to the figure eight:

$$\begin{array}{ccc} [r(\lambda)] & \in & \pi_1(r(Y)) \\ \downarrow & & \downarrow r_*^{-1} \\ [\lambda] & \in & \pi_1(Y) \\ \downarrow & & \downarrow (Y \hookrightarrow N)_* \\ [\lambda] & \in & \pi_1(N) \end{array}$$

Thus, the word $l \in \pi_1(N)$ given above is the same as $\iota_*(l') = [\lambda] \in \pi_1(N)$; multiplying it with m^j ($j = -\operatorname{lk}(l', K)$) yields a longitude. □

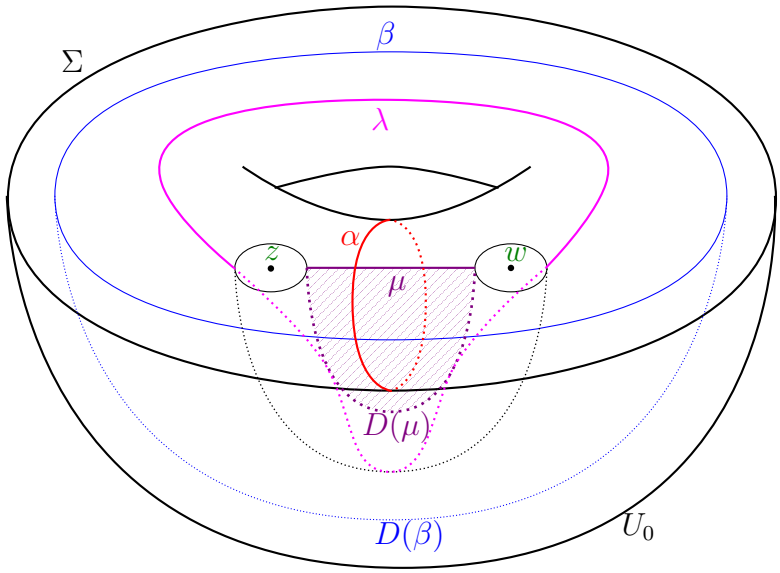

Figure 3.6: Illustration of λ in Y

Remark 3.4.20. *An explicit formula for j is $j = -A(l) \in H_1(K) \equiv \mathbb{Z}$, since we know $A(l_0) = 0$.*

The qualitative result in Lemma has been generalized to (g, b)-knots in S^3 (see for example [7], [4]); a similar proof yields the following

Proposition 3.4.21. *If $K \subset S^3$ is a (g, b)-knot with $b > 0$, then the fundamental group may be given as*

$$\pi_1(S^3 \setminus \operatorname{nd}(K)) = \langle b_1, \ldots, b_g, m_1, \ldots, m_b | r_1, \ldots, r_{g+b-1} \rangle$$

where $m_i \in \pi_1(S^3 \setminus \operatorname{nd}(K))$ are meridians, $b_j \in \pi_1(S^3 \setminus \operatorname{nd}(K))$ are arbitrary elements, and $r_k \in \langle b_1, \ldots, b_g, m_1, \ldots, m_b \rangle$ are relations.

To our best knowledge, the following conjecture is still open:

Conjecture 3.4.22 (Meridional Generator Conjecture [4])**.** *Proposition 3.4.21 is if-and-only-if, i.e. it gives a characterization of (g, b)-knots on S^3 (for $b > 0$).*

3.5 Knot Floer homology for (1,1)-knots

Heegaard Floer knot invariants are particularly appealing for (1,1)-knots, because they support doubly-pointed Heegaard diagrams with $g = 1$. In this case, Σ^g is the first symmetric power of a genus 1 surface, i.e. an ordinary torus. The chain complexes CFK^-, $\widehat{CFK}$, etc. are generated by the individual intersection points $\alpha \cap \beta$ over the appropriate module.

The boundary maps may also be described in terms of simple combinatorics, as explained by Goda, Matsuda and Morifuji in [11]. All holomorphic discs between the Lagrangian submanifolds T_α and T_β have to be immersed *bigons*. Thanks to the Riemann-Caratheodory mapping theorem, every immersed bigon can be covered by a holomorphic disk, uniquely up to reparametrization (an $\mathbb{R}$-action on the unit disk). Moreover, when working over $\mathbb{Z}$, one can obtain the correct signs by comparing the orientations of α, β and Σ in the bigon; see [11] for more details.

Following [11], let us pick a lifting $\tilde{\alpha}$ of α and $\tilde{\beta}$ of β at the universal covering map $p : \mathbb{C} \to \Sigma$. Then, $\tilde{\alpha}$ and $\tilde{\beta}$ are oriented, properly embedded lines (i.e. homeomorphic to $\mathbb{R}$). $\tilde{\alpha} \cap \tilde{\beta}$ contains a unique lifting $\tilde{x}_i$ of each intersection point $x_i \in \alpha \cap \beta$.

Lemma 3.5.1. *Let $I(\tilde{\alpha})$ and $I(\tilde{\beta})$ denote the segments of $\tilde{\alpha}$ and $\tilde{\beta}$ between $\tilde{x}$ and $\tilde{y}$, respectively.*

If $I(\tilde{\alpha}) \cap \tilde{\beta} = \{\tilde{x}, \tilde{y}\}$, then there exists a pseudo-holomorphic disk ϕ such that $\mu(\phi) = 1$ and $[\phi] \in \pi_2(\Sigma, x, y) \cup \pi_2(\Sigma, y, x)$.

Proof. Let us make the universal cover $\tilde{\Sigma}$ an almost complex manifold using the pullback $J_{\tilde{\Sigma}} = p^*(J_\Sigma)$.

Let $\tilde{\gamma} : S^1 \to \tilde{\Sigma}$ be a continuous curve traversing $I(\tilde{\alpha}) \cup I(\tilde{\beta})$. Using the condition $I(\tilde{\alpha}) \cap \tilde{\beta} = \{x, y\}$, we see that $\tilde{\gamma}$ is injective, so by the Jordan curve theorem and the Riemann–Caratheodory theorem, there exists a holomorphic disk $\tilde{\phi} : (D \subset \mathbb{C}) \to \tilde{\Sigma}$ such that $[\tilde{\phi}] \in \pi_2(\tilde{\Sigma}, \tilde{x}, \tilde{y}) \cup \pi_2(\tilde{\Sigma}, \tilde{y}, \tilde{x})$ (depending on the orientations at x and y).

Next, we compute the Maslov index of $\tilde{\phi}$. We use the formula from Lipshitz [20]: $\mu(\tilde{\phi}) = n_x([\tilde{\phi}]) + n_{x'}([\tilde{\phi}]) + e([\tilde{\phi}])$, where $[\tilde{\phi}]$ is the associated homotopy class (shadow). Since $\tilde{\phi}$ is a homeomorphism to a disk, $e([\tilde{\phi}]) = \frac{1}{2}$.

In addition, all of $\tilde{\gamma}$ and therefore all of $\tilde{\phi}(D)$ is on one side of $\tilde{\beta}$, so $[\tilde{\phi}]$ is zero on the other side of $\tilde{\beta}$. Using the fact that $\tilde{\phi}$ is injective, we have $n_{\tilde{x}}([\tilde{\phi}]) = n_{\tilde{y}}([\tilde{\phi}]) = \frac{1}{4}$.

So $\mu(\tilde{\phi}) = 1$. Let $\phi = p \circ \tilde{\phi}$. Since $p : \tilde{\Sigma} \to \Sigma$ is a local diffeormorphism that preserves the almost complex structure, we get $\mu(\phi) = 1$.

□

It is sometimes useful to consider the difference of the Maslov and Alexander gradings: the δ-grading $\delta(x) = M(x) - A(x)$ for any homogeneous element $x \in \widehat{CFK}(S^3, K)$ (or $x \in \widehat{HFK}(S^3, K)$). Let us recall a certain simplicity property for knots:

Definition 3.5.2. *A knot is called* homologically thin *(with respect to knot Floer homology) if $\widehat{HFK}(S^3, K)$ is supported in a single δ-grading.*

Quasi-alternating knots are always homologically thin [28], but there are many examples (even among reasonably small knots) that are homologically thin but not quasi-alternating. We now give a necessary condition for a $(1,1)$-knot to be homologically thin.

Theorem 3.5.3. *If $\mathcal{D}_{(1,1)}(k, r, c, s)$ represents a knot K that is homologically thin, then $s = 0$.*

Proof. Assume $s \neq 0$; we will show that K cannot be homologically thin.

Let us fix two liftings $\tilde{\beta}_0 = \tilde{\beta}$ and $\tilde{\beta}_1 \in p^{-1}(\beta)$. Consider the three connected components of $\tilde{\Sigma} \setminus (\tilde{\beta}_0 \cup \tilde{\beta}_1)$; exactly one of the components is adjacent to both of the others (the "strip", as opposed to the two "half-planes"); call it S. By choosing $\tilde{\beta}_1$ suitably (i.e. as a "neighbor" of $\tilde{\beta}$), we can ensure that $p(S) \cap \beta = \emptyset$.

Let us now examine the connected components that the closure $\bar{S}$ intersects out of $\tilde{\alpha}$. There will be $n = 2k + 1$ such components: one lifting of each arc in $\mathcal{D}$. Let us list the

liftings of the bridges: $\tilde{b}_1, \ldots, \tilde{b}_{n-2r}$, in the order as they follow on $\tilde{\alpha}$, ignoring the loops for now. As $s \neq 0$, then there exist bridges of two different kinds ("left" and "right"), there will be at least one pair of consecutive, different bridges on this list, say $\tilde{b}_i$ and $\tilde{b}_{i+1}$, with the $\tilde{\alpha}$-segment $\tilde{I}$ connecting them.

$\tilde{b}_i$ connects $\tilde{\beta}_0$ and $\tilde{\beta}_1$. Without loss of generality, we may assume its forward end (according to the direction fixed on $\tilde{\alpha}$) is a point on $\tilde{\beta}_1$. If this is the case, $\tilde{I} \cap \tilde{\beta}_0 = \emptyset$, since to reach $\tilde{\beta}_0$ from $\tilde{\beta}_1$, $\tilde{I}$ would have to contain one of the other bridges $\tilde{b}_j$. Therefore, $I(\tilde{\alpha}) = \tilde{b}_i \cup \tilde{I} \cup \tilde{b}_{i+1}$ is disjoint from $\tilde{\beta}$, and from Lemma 3.5.1, we get a pseudo-holomorphic disk ϕ with $\mu(\phi) = 1$ and $[\phi] \in \pi_2(\Sigma, x, y) \cup \pi_2(\Sigma, y, x)$, where $\tilde{x} = \tilde{b}_i \cap \tilde{\beta}_0$ and $\tilde{y} = \tilde{b}_{i+1} \cap \tilde{\beta}_0$ (and $x = p(\tilde{x})$, $y = p(\tilde{y})$ as before).

Since the direction of the bridges in the strip S changes between $\tilde{x}$ and $\tilde{y}$ on $\tilde{\beta}$, there must be a hexagonal region $H \subset S$ such that $\bar{H} \cap I(\tilde{\beta}) \neq \emptyset$. Since the lifted disk $\tilde{\phi} : D \to \tilde{\Sigma}$ is an embedding, we know that $[\phi](p(H)) \geq [\tilde{\phi}](H) = 1$. Using the fact that $e(\phi) = \frac{1}{2}$, it follows that $[\tilde{\phi}]$ has at least 2 bigon regions (with multiplicity), i.e. $n_w([\phi]) + n_z([\phi]) \geq 2$.

Comparing ϕ with the Knot Floer δ-grading, we get

$$\pm(\delta(x) - \delta(y)) = n_w([\phi]) + n_z([\phi]) - 1 \neq 0;$$

that is, the underlying knot is not homologically thin. □

Theorem 3.5.4. *There are $(1,1)$-knots with $s = 0$ that are not homologically thin (i.e. the converse of Theorem 3.5.3 is false).*

Proof. One counterexample is the knot K represented by $\mathcal{D}_{(1,1)}(5, 2, 4, 0)$, see Figure 3.7. Σ itself is shown on the left, while part of the universal cover $\mathbb{C}$ over Σ is shown on the right. The shaded region on the right is the image of a holomorphic disk ϕ of Maslov index 1, yet $n_w + n_z = 3$. Thus, the δ-gradings of the two ends of the disk differ (by 2).

Since $\widehat{\partial} = 0$ for minimal $(1,1)$-diagrams, neither of these generators of $\widehat{CFK}$ are cancelled out by taking homology, so $\widehat{HFK}$ is not homogeneous in δ-grading. In fact, the Poincaré

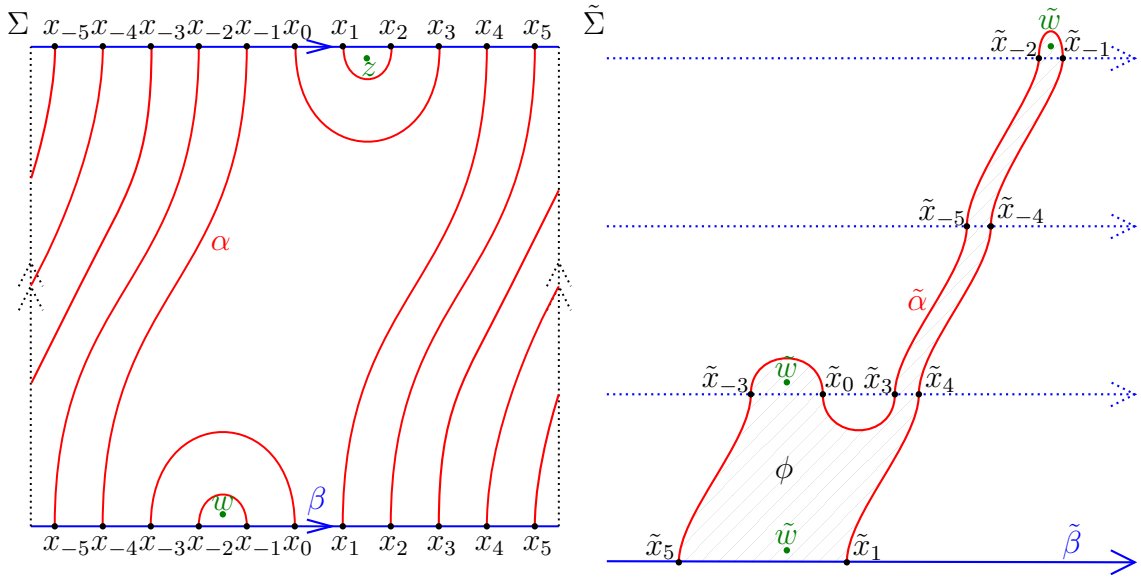

Figure 3.7: Diagram $\mathcal{D}_{(1,1)}(5,2,4,0)$ and the image of ϕ in the universal cover

polynomial of $\widehat{HFK}(S^3,K)$, as computed by our computational tools (and grouped to show δ-gradings), is as follows:

$$\begin{aligned} HFK_K(q,t) = q^7 \cdot \left((qt)^{-7} + (qt)^{-6} + (qt)^6 + (qt)^7\right) + \\ + q^5 \cdot \left((qt)^{-3} + (qt)^{-2} + (qt)^{-1} + 1 + qt + (qt)^2 + (qt)^3\right) \end{aligned}$$

□

Definition 3.5.5. *We will call a knot $K \subset S^3$* quasi-thin *if* $\mathrm{rk}\widehat{HFK}(K) = |\Delta_K(-1)|$*; in other words, $\widehat{HFK}(K)$ is in a constant δ-grading* mod 2*.*

Lemma 3.5.6. *If K is quasi-thin, then we have*

- *$g(K)$ is equal to the degree of the Alexander polynomial Δ_K;*
- *K is fibered if and only if the leading coefficient of Δ_K is ± 1.*

Proof. For a quasi-thin knot, the coefficient of t^a in $\Delta_K(t)$ is

$$\sum_{m\in\mathbb{Z}} (-1)^m \mathrm{rk}\widehat{HFK}_m(S^3,K,a) = \pm \mathrm{rk}\widehat{HFK}(S^3,K,a).$$

It is now straightforward to apply the respective results from [28] and [23]. □

Theorem 3.5.7. *If $K \subset S^3$ is represented by the $(1,1)$-diagram $\mathcal{D}_{(1,1)}(k,r,c,0)$ (i.e. $s=0$), then K is quasi-thin.*

Proof. Following Theorem 3.5.3, consider any pseudo-holomorphic disk ϕ with $\mu(\phi) = 1$. We know that $1 = 2e([\phi]) = n_w([\phi]) + n_z([\phi]) - 2[\phi](O)$, where $[\phi](O)$ is the multiplicity of the unique octagonal region. That implies $2 \nmid n_w([\phi]) + n_z([\phi])$, so $\pm(\delta(x) - \delta(y)) = n_w([\phi]) + n_z([\phi]) - 1 \equiv 0 \mod 2$.

Since any two generators of $\widehat{HFK}(K)$ may be connected by pseudo-holomorphic disks ϕ with $\mu(\phi) = 1$, we see that the δ-grading has constant parity. □

Corollary 3.5.8. *If $K \subset S^3$ is represented by the $(1,1)$-diagram $\mathcal{D}_{(1,1)}(k,r,c,0)$ (i.e. $s=0$), then*

- *$g(K)$ is equal to the degree of the Alexander polynomial Δ_K;*
- *K is fibered if and only if the leading coefficient of Δ_K is ± 1.*

3.6 (1,1)-knots with trivial Alexander polynomial

Using the computational tools at our disposal, we found a parametric class of $(1,1)$-knots with trivial Alexander polynomial, as well as more exotic "sporadic" examples.

Theorem 3.6.1. *Consider the $(1,1)$-diagrams $\mathcal{D}_n = \mathcal{D}_{(1,1)}(16n-1, 12n-1, 12n-1, -1)$ for $n \in \mathbb{N}$, and the distinct $(1,1)$-knots K_n that they define. If $n \leq 20$, we have computationally verified:*

- *The Alexander polynomial is trivial: $\Delta_{K_n}(t) = 1$ for all n.*
- *$\tau(K_n) = -1$ for all n.*

- *The bi-graded* $\widehat{HFK}$ *invariant is as follows:*
  $$HFK_{K_n}(q,t) = \big(n\cdot(qt)^{-2} + 4n\cdot(qt)^{-1} + \quad 6n \quad + 4n\cdot qt + n\cdot(qt)^2\big) +$$
  $$q\cdot\big(n\cdot(qt)^{-2} + 4n\cdot(qt)^{-1} + (6n-1) + 4n\cdot qt + n\cdot(qt)^2\big)$$
- *Figure 3.8 shows a planar diagram for* K_n*; in particular, the crossing number is at most* $14+n$*.*

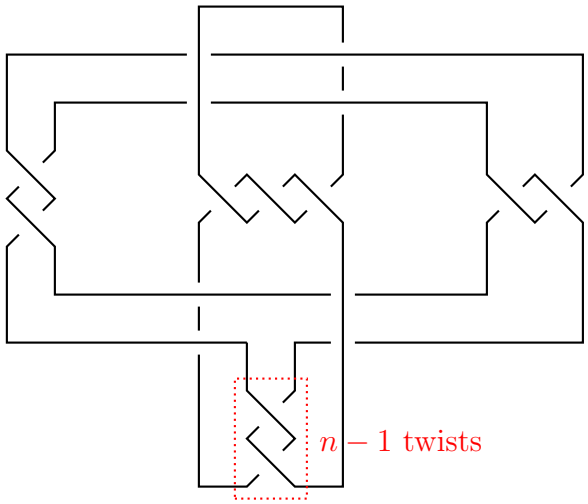

Figure 3.8: Planar diagram for K_n ($n=3$ is shown)

Remark 3.6.2. *For* $n=1$*, the crossing number is in fact* 13*; we believe that the knot* $K_1 = 13n_{1496} = [4,2;3,2;2-] = [5,-2;3,2;2-]$ *has the least crossing number among* $(1,1)$*-knots with* $\Delta = 1$*.*

We conjecture that Theorem 3.6.1 is true for all $n \in \mathbb{N}$. This would also imply the following

Conjecture 3.6.3. *There are infinitely many* $(1,1)$*-knots that are topologically slice, but not smoothly slice.*

The above examples had genus $g=2$, and the structure of $\widehat{HFK}$ was very simple, with all generators in only 10 (Alexander, Maslov) bigradings. As we increase the Heegaard Floer rank $\operatorname{rk}\widehat{HFK}(S^3,K) = 2k+1$, more complicated examples emerge. Figure 3.9 shows the dimensions of $\operatorname{rk}\widehat{HFK}(S^3,K)$ in each bigrading for the diagram $\mathcal{D}_{(1,1)}(63,23,39,-33)$.

m \ a	-4	-3	-2	-1	0	1	2	3	4
5									1
4								4	1
3							6	3	
2						8	4		
1					9	5	2	1	
0				8	**6**	4	4		
-1			6	5	4	7			
-2		4	4	4	8				
-3	1	3	2	7					
-4	1		4						
-5		1							

Figure 3.9: $(a, m) \to \operatorname{rk} \widehat{HFK}_m(S^3, K, a)$ for $K \sim \mathcal{D}_{(1,1)}(63, 23, 39, -33)$

Interestingly, we did not find any $(1,1)$-knots K with $\Delta_K(t) = 1$ and genus one. In addition, all examples had $k \equiv 0, -1 \mod 16$, or in other words, $\operatorname{rk} \widehat{HFK} \equiv \pm 1 \mod 32$.

3.7 Computational Tools and Proof of Theorem 3.3.1

Throughout this section, the words *small knot* will stand for any knot that has a planar diagram with 12 or fewer crossings.

We simply check all $(1,1)$-diagrams that are, in a certain sense, "small enough" to possibly represent small knots, and identify those that indeed do.

To do this, we need to solve the following problems:

- List all $(1,1)$-diagrams that might represent small knots
- Of this list, identify $(1,1)$-diagrams that do actually represent small knots
- Prove that all the other diagrams are inequivalent to all small knots

3.7.1 Listing all candidate $(1,1)$-diagrams

For this step, we use Baldwin and Gillam's computations of $\widehat{HFK}$ for knots up to 12 crossings.

Due to Corollary 3.4.5, if a knot K is represented by $(1,1)$-diagram $\mathcal{D}_{(1,1)}(k,r,c,s)$ (with $|\alpha \cap \beta| = 2k+1$), we know that $2k+1 = \operatorname{rk} \widehat{HFK}(S^3,K)$, which means the parameter k is fixed. Using the big O (ordo) notation from complexity theory, this leaves $O(k^3)$ possibilities for the other three parameters.

Furthermore, if K is homologically thin, we know that any diagram $\mathcal{D}_{(1,1)}(k,r,c,s)$ representing it must have $s=0$ (Theorem 3.5.3), leaving only $O(k^2)$ possibilities. This is especially useful as homologically thin knots (especially alternating knots) tend to have much higher total knot Floer rank $\operatorname{rk} \widehat{HFK}$ than non-thin knots with the same crossing number.

3.7.2 Excluding $(1,1)$-diagrams that do not represent small knots

Conveniently, we already have one obstruction: from Baldwin and Gilam, we already know $\widehat{HFK}$ for small knots, and we can easily compute $\widehat{HFK}$ for $(1,1)$-diagrams.

However, $\widehat{HFK}$ is far from being a complete knot invariant; we need a more powerful method to eliminate false matches. The fundamental group $\pi_1(S^3 \setminus K)$ is easy to calculate from both a knot diagram and a $(1,1)$-diagram, and it is suitably powerful; by Gordon and Luecke [12], it differentiates prime knots up to orientation.

Definition 3.7.1. *In this section, the term* framed group *will refer to a group G with a distinguised pair of elements $(m,l) \in G \times G$, fixed up to an internal automorphism (conjugation).*

Remark 3.7.2. *If $K \subset S^3$ is an oriented knot, a peripherial system of K (i.e. the fundamental group $G = \pi_1(S^3 \setminus G)$ with a meridian m and longitude l) is naturally equipped with a framed group structure. We can observe that $ml = lm$ and in $G/[G,G] = H_1(S^3 \setminus K) \equiv \mathbb{Z}$, $l[G,G] = 1$ and $m[G,G] = 0$.*

If knots K_1 and K_2 are equivalent, then there is a framed group isomorphism $i : \pi_1(K_1) \to \pi_1(K_2)$ (preserving the distinguished elements: $i(m_1) = m_2$ and $i(l_1) = l_2$). Unfortunately, in general it is very difficult to verify whether such i exists. Thus, we settle for examining the representations of $G_j = \pi_1(K_j)$ in suitably chosen finite groups H.

Definition 3.7.3. *The* signature *of a framed group $G, (m, l)$ on a finite group H is a function $s_G : H \times H \to \mathbb{Z}^+$ such that*

$$s_G(\mu, \lambda) = \#\left\{f : G \to H | \mu = f(m), \lambda = f(l)\right\}.$$

Remark 3.7.4. *Clearly, $s_G(\mu, \lambda) = s_G(\alpha\mu\alpha^{-1}, \alpha\lambda\alpha^{-1})$ for $\alpha \in H$. Furthermore, if G is a knot's fundamental group with meridian m and longitude l, then $s_G(\mu, \lambda) \neq 0$ only if μ and λ commute.*

Remark 3.7.5. *The isomorphism type of $G = \pi_1(S^3 \setminus K)$ as a group cannot differentiate between a knot K and its mirror image $\overline{K}$ or reverse $r(K)$. However, $G, (m, l)$ as a framed group is – in general – inequivalent when we change orientations.*

If we choose a group H where $h \sim h^{-1}$ does not hold for all elements $h \in H$ (for instance, the affine group on the line $H = A_1(GF(p))$ for a prime $p \geq 5$), the signature may be different for the different orientations of the same unoriented knot.

Nevertheless, we do not rely on the orientations of m and l in our computations.

Since the Abelianization $G/[G, G] \equiv \mathbb{Z}$ is the same for all fundamental groups G, this signature only carries information if H is non-Abelian. We exclude all false matches by verifying signatures in finite non-Abelian groups H, including:

- Dihedral groups D_k $(k \leq 50)$
- Alternating groups A_k $(k \leq 6)$

3.7.3 Identifying small knots represented by the remaining $(1,1)$-diagrams

The classification is complete if we can show that all remaining $(1,1)$-diagrams on the list of candidates are equivalent to a small knot. To do this, we use a heuristic algorithm which manipulates planar diagrams directly.

Given a planar diagram in S^2 for a knot (or link) in S^3, one may subdivide the planar diagram into *overpasses* (segments which only contain over-crossings) and *underpasses* (only under-crossings).

Definition 3.7.6. *An* overpass move *on a planar diagram consists of removing an overpass and connecting its ends with a new overpass in an arbitrary manner; mutatis mutandis for an* underpass move.

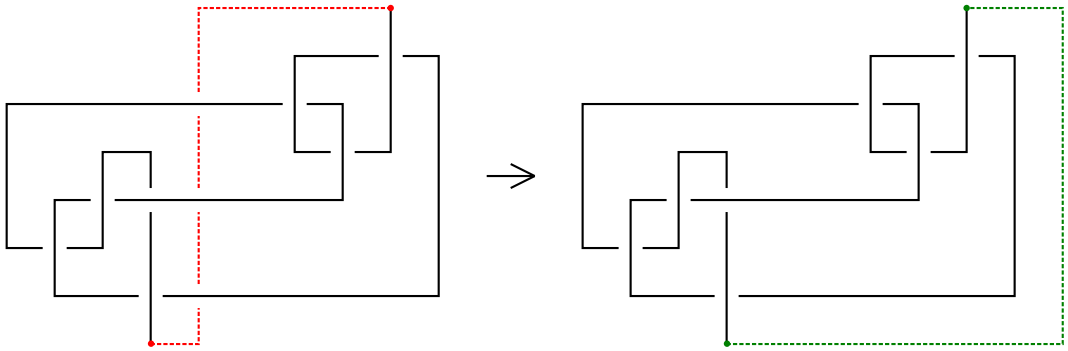

Figure 3.10: Example: Underpass move

See Figure 3.10 for an example of an underpass move. The knot shown is the hard-to-simplify[1] unknot *The Culprit* from [15].

Clearly, such pass moves preserve the isotopy type of a link. Reidemeister moves I–III can be regarded as pass moves, so Reidemeister's theorem easily implies the

Corollary 3.7.7. *Two planar diagrams in S^2 represent the same link in S^3 if and only if they can be connected via a sequence of pass moves.*

[1] As [15] shows, if we only use the classical Reidemeister moves, we have to increase the crossing number of this diagram from 10 to 12 before reaching a diagram with fewer than 10 crossings.

To identify the knots represented by $(1,1)$-diagrams, first we simply construct an arbitrary (and – in terms of crossing number – quite wasteful) planar diagram for these knots.

Then, we use a greedy algorithm to reduce the number of crossings: whenever a pass may be replaced by a pass with fewer crossings, so we do. This algorithm will not result in the minimal crossing number diagram in general. The only case where we can be confident to have reached the minimal crossing number is alternating diagrams:

Lemma 3.7.8. *If an* alternating *diagram in S^2 (representing a link L in S^3) is such that no pass move decreases the crossing number, then the diagram implements the (minimum) crossing number of L.*

Proof. An alternating diagram D minimizes the crossing number for L if no simplifying "flype" move is possible (see e.g. [19]), i.e. if no region of $S^2 \setminus D$ is diagonally adjacent to itself at a crossing.

Such a crossing would, in turn, allow us to replace a pass of 1 crossing with a pass of 0 crossings (see Figure 3.11). (Indeed, this is the only type of pass move to decrease the number of crossings in an alternating diagram, as all passes have at most 1 crossing). □

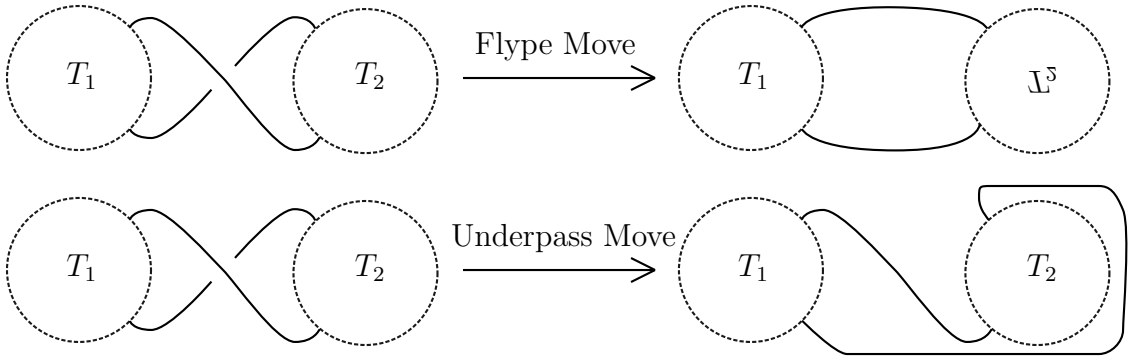

Figure 3.11: Flype Move and similar Underpass Move

To make the algorithm slightly more ambitious, we do not stop instantly if there is no single pass move that decreases the crossing number (unless the diagram is alternating, as discussed above). Instead, we try replacing a *maximal* pass with an alternative pass of the

same number of crossings randomly, and try greedy elimination again. If this fails for a given number of attempts, we stop.

There is no guarantee that this process finds a minimal crossing diagram for a general knot, but it performs well enough for our purposes: for each candidate $(1,1)$-diagram, we were able to prove either that it is inequivalent to all small knots, or simplify it to a small knot.

Using the notations introduced in Corollary 3.4.7, the following table lists one possible choice of parameters for each non-Montesinos $(1,1)$-knot up to 12 crossings (where knot K is represented by $\mathcal{D}_{(1,1)}(k,r,c,s)$).

K	k	r	c	s	K	k	r	c	s	K	k	r	c	s
10_{161}	6	3	-3	3	$11n_{96}$	12	6	6	3	$11n_{111}$	11	6	6	-3
$11n_{135}$	10	5	-5	3	$12n_{352}$	20	10	10	3	$12n_{370}$	13	6	-6	-1
$12n_{371}$	13	10	-10	3	$12n_{374}$	17	15	3	-1	$12n_{404}$	14	7	7	1
$12n_{433}$	18	9	9	5	$12n_{446}$	19	10	10	-3	$12n_{464}$	23	18	6	-3
$12n_{483}$	24	18	6	3	$12n_{487}$	13	6	6	-7	$12n_{488}$	10	6	-6	1
$12n_{500}$	25	22	16	0	$12n_{501}$	24	21	4	0	$12n_{502}$	7	4	-4	-2
$12n_{503}$	18	15	3	-2	$12n_{552}$	20	11	10	3	$12n_{579}$	20	10	-10	5
$12n_{591}$	7	4	-4	-3	$12n_{594}$	18	10	-9	-5	$12n_{624}$	18	9	9	-7
$12n_{650}$	24	18	6	-5	$12n_{749}$	7	3	3	4	$12n_{851}$	14	7	7	-3

Note that for most knots, there are multiple options, e.g. (k,r,c,s) typically change when the roles of the α- and β-curve are reversed.

Chapter 4

A new class of multi-pointed knot Heegaard diagrams

In [34], Sarkar and Wang introduced *nice diagrams*, a class of Heegaard diagrams where every region of $\Sigma \setminus (\alpha_1 \cup \cdots \cup \alpha_g) \setminus (\beta_1 \cup \cdots \cup \beta_g)$ that is not a bigon or a rectangle (i.e. has more than 4 sides) contains a basepoint. For these diagrams, one can compute $\widehat{HFK}$ in a combinatorial fashion, as all pseudo-holomorphic disks contributing to the boundary map $\hat{\partial}$ project to embedded bigons or rectangles on Σ. Their definition applies to multi-pointed and link Heegaard diagrams as well.

Let $R_\alpha = \Sigma \setminus \cup_{\alpha_i \in \boldsymbol{\alpha}} \alpha_i$ denote the complement of the α-curves in a diagram, and similarly, R_β denote the complement of the β-curves. We will refer to connected components of R_α as *components*, and connected components of $R_\alpha \cap R_\beta$ as *regions*.

If *all* of the regions are bigons or rectangles, then even the stronger invariant HFK^- can be described combinatorically. This is advantageous for certain applications, such as analyzing surgeries along links. In this case, the Euler characteristic of Σ is nonnegative; therefore, Σ is either a torus or S^2.

When Σ is a torus, all regions are rectangles. If the underlying manifold is S^3, one obtains the well-studied *grid diagrams*, and the resulting combinatorial theory (Grid Homology)

provides a self-contained combinatorial construction of Knot Floer homology for links in S^3 [21]. (The underlying manifold may also be a different lens space, see [1].) One drawback of Grid Homology is that the number of generators in the chain complex is $k!$ for a $k \times k$ grid diagram; larger grids are not practical for computational purposes.

We are investigating the case when $\Sigma = S^2$. In this case, we have $k-1$ each of α and β-curves, and k pairs of base points. Each component of R_α contains one basepoint w_i and one z_j, and similarly for R_β.

4.1 Perfect $(0,k)$-diagrams

Let us introduce some shorthands for Heegaard diagrams on S^2:

Definition 4.1.1. *A* $(0,k)$-diagram *is a multi-pointed link Heegaard diagram* $(\Sigma, \boldsymbol{\alpha}, \boldsymbol{\beta}, \boldsymbol{z}, \boldsymbol{w})$, *where* $\Sigma = S^2$, $|\boldsymbol{\alpha}| = |\boldsymbol{\beta}| = k-1$, *and* $\alpha_i \pitchfork \beta_j \ \forall i, j$.

Each $(0,k)$-diagram represents a link in S^3. We are seeking a very restricted class of these diagrams:

Definition 4.1.2. *A* $(0,k)$*-diagram is called a* perfect $(0,k)$-diagram *if each connected region of* $R_\alpha \cap R_\beta$ *is a bigon or a rectangle.*

If a link can be represented by a perfect $(0,k)$-diagram, then the Knot Floer homology generators are $(k-1)$-tuples; when k is much smaller than the grid size for the link, the perfect $(0,k)$-diagram is likely to be computationally more tractable.

Let us name some intermediate steps to perfect $(0,k)$-diagrams:

Definition 4.1.3. *In a* $(0,k)$*-diagram, we say that the* α*-curves (respectively, the* β*-curves) are* parallel *if each component of* R_α *(or respectively,* R_β*) is homeomorphic to either a disk or an annulus. We say that the* $(0,k)$*-diagram is* parallel *if both the set of its* α*-curves and the set of its* β*-curves is parallel.*

Definition 4.1.4. *In a $(0,k)$-diagram, we say that the α-curves are* close parallel *if all α_i $(1 \leq 1 \leq k-1)$ are sections of a tubular neighborhood $N_{\boldsymbol{\alpha}} : S^1 \times (0,1) \to \Sigma$ that is transverse to all β-curves. We say that the $(0,k)$-diagram is* close parallel *if both the set of its α-curves and the set of its β-curves is close parallel.*

Note that we can tell whether the α-curves are parallel without considering the β-curves, but the same is not true for the close parallelism. The close parallel property is indeed strictly stronger:

Lemma 4.1.5. *The α-curves are close parallel in a $(0,k)$-diagram if and only if they are parallel, and each annulus component of R_α only contains rectangular regions of $R_\alpha \cap R_\beta$ (unless the β-curves do not intersect the α-curves at all, a denegenrate case).*

Proof. Assume that the α-curves are close parallel. Since they are non-intersecting, they follow in the same well-defined order across all fibers of $N_{\boldsymbol{\alpha}}$. If we use this order to index them, one can see that the extreme curves α_1 and α_{k-1} enclose one disk each by the Jordan curve theorem, and there are $k-2$ annuli between α_j and α_{j+1} $(1 \leq j \leq k-2)$. Thus, the α-curves are parallel. Unless these annular components are disjoint from the β-curves, all regions within are created between two transverse intersections of β-curves with $N_{\boldsymbol{\alpha}}$, which produce rectangles.

Now assume that the α-curves are parallel and all annulus components of R_α comprise of rectangular regions. Let us index the α-curves starting from one of the disk regions, such that each annulus is bounded by $\alpha_j \cup \alpha_{j+1}$ for some $1 \leq j \leq k-2$. The β-sides of the rectangles line up to form β-segments $\beta_1^S, \ldots, \beta_n^S$, which follow in the same cyclical order on each α-curve; overall, the annuli compose into a rectangular grid.

We may construct the tubular neighborhood $N_{\boldsymbol{\alpha}}$ as follows: first define $N_{\boldsymbol{\alpha}}$ in the intersection points respecting the grid:

$$N_{\boldsymbol{\alpha}}\left(\frac{i}{n} + \mathbb{Z}, \frac{j}{k}\right) = \beta_i^S \cap \alpha_j$$

Then, extend $N_{\boldsymbol{\alpha}}$ continuously such that its restrictions are homeomorphisms $\left(\frac{i}{n}+\mathbb{Z}\right)\times(0,1)\to\beta_i^S$ and $S^1\times\frac{j}{k}\to\alpha_j$. Finally, extend $N_{\boldsymbol{\alpha}}$ to map the grid rectangles homeomorphically onto the rectangular regions, and the open rectangles to narrow strips transverse to the β-curves. □

Corollary 4.1.6. *A perfect $(0,k)$-diagram is also close parallel.*

Proof. Since the diagram is perfect, all components of R_α are composed of bigons and rectangles – both of non-negative Euler measure. Thus, all components C have $\chi(C)\geq 0$, i.e. they are disks or annuli. Therefore, all perfect $(0,k)$-diagrams are parallel; combined with Lemma 4.1.5, they also have to be close parallel. □

4.2 Parallelizing $(0,k)$-diagrams

If a link $L\subset S^3$ is represented by a $(0,k)$-diagram, then it has a k-bridge representation (over S^2 equivalently, $\mathbb{R}^2$). The inverse is also true:

Observation 4.2.1. *Any k-bridge link $L\subset S^3$ can be represented by some $(0,k)$-diagram.*

Proof. Start with an oriented k-bridge representation over $\Sigma=S^2$ with over-arcs o_i and under-arcs u_i $(1\leq i\leq k)$. The base-points w_j are the points where under-arcs change to over-arcs; z_j the opposite.

Let α_i be a contour of o_i $(1\leq i\leq k-1)$, close enough to o_i that the α_i's are disjoint from the o_i's and one another (see Figure 4.1). Similarly, let β_i be a contour of u_i $(1\leq i\leq k-1)$. The resulting diagram $(\Sigma,\boldsymbol{\alpha},\boldsymbol{\beta},\boldsymbol{z},\boldsymbol{w})$ represents L. □

We would like to know whether a link $L\subset S^3$ can be represented by a *perfect* $(0,k)$-diagram. If there is no restriction on k, this is easy; in fact:

Observation 4.2.2. *If the link $L\subset S^3$ has a grid diagram of grid number k, then it also has a perfect $(0,k)$-diagram; specifically, the curves are $k-1$ parallel copies each of two circles*

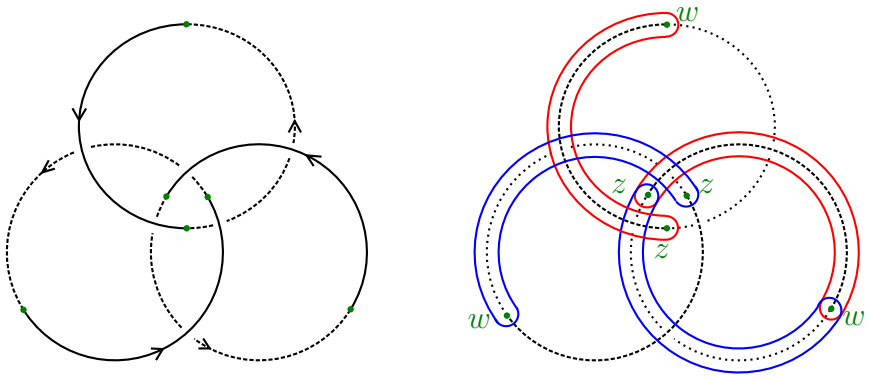

Figure 4.1: Constructing a $(0,k)$-diagram from a k-bridge presentation

intersecting transversely in two points (the perfect $(0,k)$*-diagram has* $2(k-1)^2$ *intersection points in total). In this sense, perfect* $(0,k)$*-diagrams generalize grid diagrams.*

A more interesting question is whether we can decrease k. Can a k-bridge link $L \subset S^3$ always be represented by a perfect $(0,k)$-diagram? We attempt to answer this question. The current Section 4.2 proves some partial results on this front, while the following Section 4.3 documents our efforts to settle the issue.

To simplify the picture, we would like to concentrate on the α- and β-curves and disregard the base points for the moment. Let us examine which of the classical Heegaard moves may we perform.

Observation 4.2.3. *Consider a multi-pointed Heegaard diagram* $\mathcal{D}$ *and its copy with base points erased,* $\mathcal{D}_0$*.*

- all *handle slides that may be performed on* $\mathcal{D}_0$ *may be lifted to a handle slide on* $\mathcal{D}$*;*
- *of the isotopies on* $\mathcal{D}_0$*, those which only involve "birth" of intersection points* $\alpha \cap \beta$ *can always be lifted to* $\mathcal{D}$*; those that also involve "death" of intersection points might not.*

Definition 4.2.4. *An* elementary isotopy *of a Heegaard diagram is one whose ends only differ locally, as shown in the Figure 4.2. The elementary isotopy is* increasing *when the number of intersection points is increased by* 2 *and* decreasing *otherwise.*

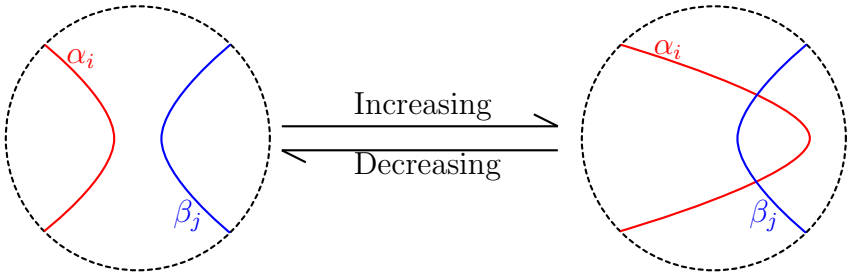

Figure 4.2: Elementary isotopies

Theorem 4.2.5. *Any $(0, k)$ diagram can be transformed by a sequence of handle slides such that the α-curves (and the β-curves) become parallel.*

Proof. Let us define a graph $\mathcal{A}$ whose vertices are components of R_α, and its edges are the α-curves. An edge α_j is incident to a component C if $\alpha_j \subset \partial C$. Observe that the α-curves are parallel if and only if $\mathcal{A}$ is a path graph. We claim that $\mathcal{A}$ is always a tree. (Note that we do not assume – but do prove – that $\mathcal{A}$ is a simple graph).

Indeed, by induction on k: for $k = 1$, there is a single vertex (Σ) and no edge. For $k = l+1$, consider the curve α_l. Since all components are open sets in $\Sigma = S^2$, there are two different components on either side of α_l. If we erase α_l, the two components merge, which amounts to an edge contraction in $\mathcal{A}$. By induction, $\mathcal{A}$ becomes a tree if one of its edges is contracted; therefore, $\mathcal{A}$ is a tree itself.

Now, let us examine how $\mathcal{A}$ changes through a handle slide: we slide α_i through α_j along an arc γ (see Figure 4.3). Since $int\gamma$ is disjoint from the α-curves, it is entirely in some component C_1; thus, α_i and α_j (as edges of $\mathcal{A}$) share a common end C_1. Let C_2 and C_3 be their other ends respectively. As the Figure illustrates, the handle slide changes the "cherry" $C_2 - C_1 - C_3$ into another position $C_1' - C_2' - C_3$ (we will identify $C_1 \sim C_1'$ and $C_2 \sim C_2'$ as verices of $\mathcal{A}$), leaving all other edges in the graph intact. Since only finitely many base points are forbidden from γ, all such "cherry moves" on $\mathcal{A}$ can be implemented by handle slides.

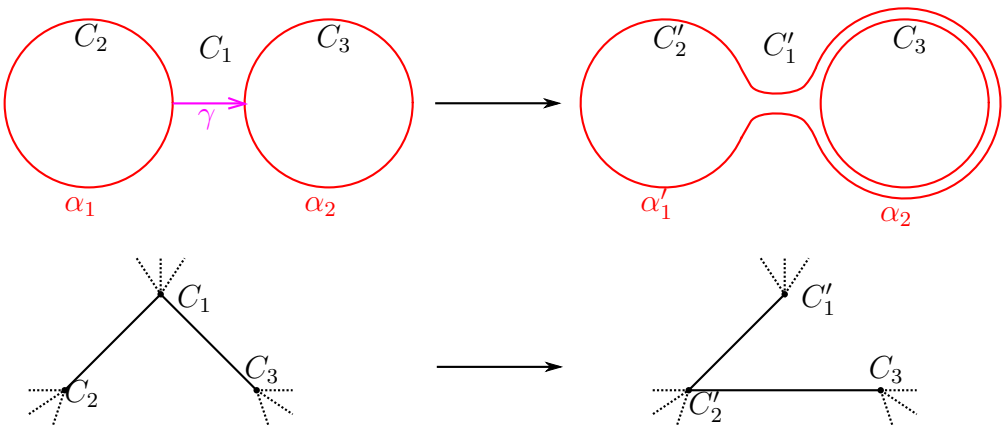

Figure 4.3: Handle slide and Cherry move

To make the α-curves parallel, we have to use "cherry moves" to transform $\mathcal{A}$ into a path graph. Assume we are not done yet: then there exists a vertex C such that $\deg C \geq 3$. Let D be one of its neighbors, and $C = C_0, C_1, \ldots, C_n$ a path from C disjoint from D such that $\deg C_n = 1$. Now, perform n handle slides to effect the cherry moves $D - C_0 - C_1 \to D - C_1 - C_0, \ldots, D - C_{n-1} - C_n \to D - C_n - C_{n-1}$.

At the end of these moves, $\deg C_0$ is decreased by 1, $\deg C_n$ is increased by 1, and all other degrees are unchanged. Importantly, the number of leaves in the tree $\mathcal{A}$ falls by 1. Thus, by repeating this procedure finitely many times, we obtain a path graph. □

Theorem 4.2.6. *Let $\mathcal{D}$ denote a parallel $(0, k)$ diagram. There exists a sequence of increasing isotopies that transforms $\mathcal{D}$ into a diagram $\mathcal{D}'$ where the α-curves are close parallel. Furthermore, if the β-curves are already close parallel, one may choose isotopies that preserve this property as well.*

Proof. Conceptually, we achieve our goal by using isotopies to "push out" all the "irregularity" to the disk components of R_α.

To define said "irregularity", recall the concept of β-segments (connected components of $\bigcup \beta \setminus (\bigcup \alpha)$) and their classification into *bridges* (that connect different α-curves) and *loops* (that return to the same α-curve). Let us define the *irregularity* (α-irregularity) of a parallel diagram $\mathcal{D}$, $irr_\alpha(\mathcal{D})$, as the number of β-loops that lie in the annulus components of R_α. If

$irr_\alpha(\mathcal{D}) = 0$, then the α-curves are close parallel. If we can find a way to decrease $irr_\alpha(\mathcal{D})$ in all other cases, the proof is concluded by induction.

Let us introduce a self-indexing Morse fuction $2f : \Sigma \to [0, 2]$ such that f only has two critical points (one in each bigon component of R_α), and the α-curves are niveau sets of f: $\alpha_j = f^{-1}\left(\frac{j}{k}\right)$, $1 \leq j \leq k-1$; as usual, we think of f as a height function. We may assume that f is still a Morse function when restricted to each β-curve, and it has at most one critical point on each β-segment (one per β-loop and zero per β-bridge). We can now further classify β-loops as *downward* and *upward* (depending on whether the respective critical point is of index 0 or 1). Without loss of generality, let us concentrate on eliminating downward β-loops.

Let us pick a β-loop β_0^S in the annuli regions of R_α such that the height of its lowest (critical) point x_0 is minimal. We claim there is a continuous path $\gamma : \left[\frac{1}{k} - \varepsilon, f(x_0)\right] \to \Sigma$ such that $f \circ \gamma = \mathrm{id}$ and $\mathrm{Im}\, f \cup \beta = \{x_0\}$; in words, a downward path that connects the loop β_0^S to a disk component of R_α, not going through any other β-segment.

To obtain this γ, let us first pick an arbitrary γ_0 that may intersect other β-segments (for example, the downward flow line from x_0 after introducing an arbitrary Riemannian metric on Σ). If γ_0 does not intersect any β-segment after leaving x_0, we are done. Otherwise, we obtain γ by following γ_0 until just before its first intersection with a β-segment, then tracing the β-curve that γ_0 hits downward (see Figure 4.4). The only way we could get stuck is a critical point of index 0 on the β-curve, but this can only happen in the disk component because of the minimailty of $f(x_0)$.

Having identified γ, we now perform a finger move of β_0^S along γ; this comprises $j-1$ increasing elementary isotopies if β_0^S connects to α_j. We created $2(j-1)$ new β-bridges and a β-loop in a disk component of R_α, but eliminated a β-loop in an annulus component, decreasing $irr_\alpha(\mathcal{D})$ by 1, thus closing the proof by induction.

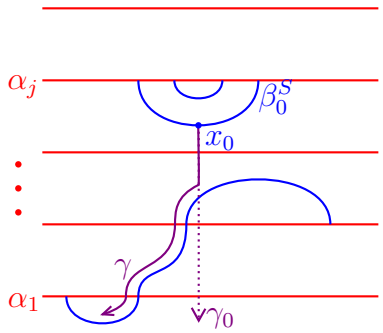

Figure 4.4: Eliminating a downward β-loop β_0^S

If the β-curves are already close parallel, we perform the same steps on a diagram with only one β_j shown, with the understanding that each finger move is performed upon all the $k-1$ close parallel copies of the β-arcs simultaneously. □

Piecing together the results above, we get the following

Theorem 4.2.7 (Parallelization)**.** *Given a $(0,k)$-diagram $\mathcal{D}$ for a link $L \subset S^3$, there exists a sequence of handle slides and isotopies (not crossing any base point) on $\mathcal{D}$ such that the resulting diagram $\mathcal{D}'$ is a close parallel $(0,k)$-diagram. In particular, k has not changed from $\mathcal{D}$ to $\mathcal{D}'$.*

4.3 Constructing perfect $(0,k)$-diagrams

In this section, we present some avenues of attack that we explored in an attempt to prove the following Conjecture:

Conjecture 4.3.1 (Geometric Conjecture about k-bridge links)**.** *For each oriented link $L \subset S^3$ that is k-bridge on $\Sigma = S^2$, there exists a* perfect $(0,k)$*-diagram representing L.*

Conjecture 4.3.1 is trivially true for $k \leq 2$. Our efforts to disprove Conjecture 4.3.1 yielded no result. If it does turn out to be false, it would still be interesting whether it may be true for $k = 3$.

To avoid complications with handle slides and stabilizations/destabilizations, we focused on studying the (stronger) Combinatoric Conjecture:

Conjecture 4.3.2 (Combinatoric Conjecture about perfect $(0,k)$-diagrams)**.** *Every* $(0,k)$*-diagram* $\mathcal{D}$ *can be transformed to a* perfect $(0,k)$*-diagram using only increasing isotopies.*

By Theorem 4.2.7, we may assume that the $\mathcal{D}$ is close parallel. This means that to prove Conjecture 4.3.2, it would be enough to show that a diagram *one* α and *one* β-curve may be transformed to a perfect diagram by only increasing isotopies.

Definition 4.3.3. *A* bicycle *consists of a pair of smooth simple curves* $\alpha : S^1_\alpha \to S^2$ *and* $\beta : S^1_\beta \to S^2$ *such that* $\alpha \pitchfork \beta$ *are transverse, up to orientation-preserving*[1] *diffeomorphisms of* S^1_α, S^1_β *and* S^2*.*

Perfectness, as well as elementary increasing and decreasing isomorphisms can be defined for bicycles in the same way as they are for $(0,k)$-diagrams. For every bicycle, there is an equal number of positive and negative intersection points $\operatorname{Im}\alpha \cap \operatorname{Im}\beta$; denote this number as $|B|$ for a bicycle B.

Conjecture 4.3.2 would follow from the following simplified form:

Conjecture 4.3.4 (Combinatoric Conjecture about bicycles)**.** *Every bicycle can be transformed into a perfect bicycle by only increasing isotopies.*

Remark 4.3.5. *The relation "Bicycle* B_1 *can be transformed into* B_2 *by a sequence of increasing isotopies" (denoted by* $B_1 \leq B_2$*) defines a partially-ordered set on the set* $\mathcal{B}$ *of all bicycles. Conjecture 4.3.4 can be reformulated as follows: perfect bicycles cover all of* $\mathcal{B}$*.*

One approach we tried is reverse construction: starting from a given perfect bicycles, what bicycles can we get through a series of decreasing isotopies? A computational partial result:

Theorem 4.3.6. *All bicycles* B *with* $|B| \leq 8$ *(i.e.* $|\operatorname{Im}\alpha \cap \operatorname{Im}\beta| \leq 16$*) are covered by a perfect bicycle.*

[1] One may also consider unoriented bicycles, where we allow any diffeomorphism, as well as swapping α and β. This mainly serves computational purposes, as it reduces the number of different bicycles of a given size by up to 2^4 (i.e. an action of the group $Z_2 \times D_4$.)

To quantify how much the bicycle has to grow to become perfect, let us denote the worst case by

$$p(n) = \max_{|B|\leq n, B\in\mathcal{B}} \left(\inf_{P\geq B, P\text{perfect}} |P| \right).$$

The known values of $p(n)$ are as follows:

n	1	2	3	4	5	6	7	8	9
$p(n)$	1	2	5	8	13	18	25	36	≥ 42

4.4 Geometry of perfect $(0, k)$-diagrams

We show that α-and β-curves in a perfect $(0, k)$-diagrams follow a quite rigid structure.

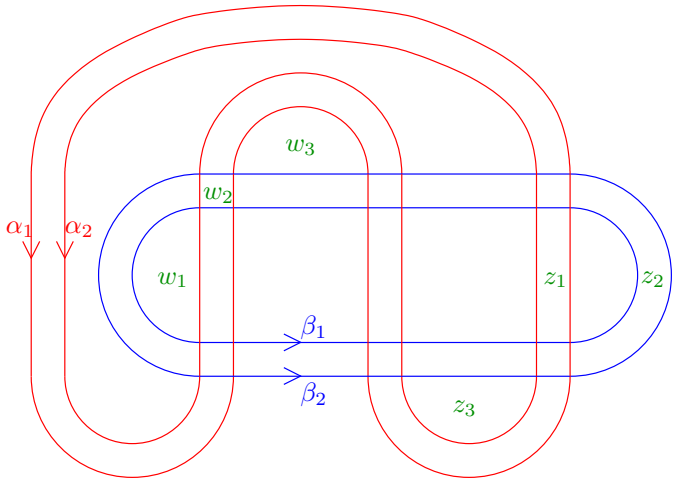

Figure 4.5: Example – Perfect $(0, 3)$-diagram representing the $(3, 4)$ torus knot (also known as 8_{19}); $p = 3,\ q = 1$

Theorem 4.4.1. *(Structure of perfect $(0, k)$-diagrams.)*

(i) $k = 2$: by cutting a perfect $(0, 2)$-diagram along its unique β-curve, one obtains two discs with p parallel α-chords each, rotated by q intersection points in the positive direction (for some integers p and q). The numbers p and q are relatively prime, and they determine the $(0, 2)$-diagram up to homeomorphism. If one places basepoints in each of the 4 bigons appropriately, the link represented is a rational (2-bridge) link with determinant p.

(ii) $k \geq 3$: The α and β-curves of a perfect $(0, k)$-diagram may be obtained as $k - 1$ close

parallel copies (situated in transverse tubular neighborhoods) of the respective curves of a perfect $(0,2)$*-diagram.*

Proof. (i) Let the integer p denote half of the number of intersections of the α- and β-curves. We can describe both components of R_β up to oriented homeomorphism: since the diagram is perfect, there must be exactly two bigons connected by a path of $p-1$ rectangles on each side.

The only piece of information missing to describe the diagram is how to glue the two R_β-components along β, that is, how to match up the intersection points $\alpha \cap \beta$, i.e. by how many intersection points to rotate the boundary β. This is described by a number $q \in \mathbb{Z}_p^\times$ (i.e. q as an integer is defined mod p and $GCD(q,p)=1$), where the latter condition ensures that the α-segments compose into a single connected α-curve. Note that q and $-q$ define mirror-symmetric diagrams, and we do not need to distinguish between the components of R_β to get a well-defined q.

If we place a base point in each of the 4 bigons, we get the Heegaard diagram for a 2-bridge link $L \sim q'/p'$ (a knot if p is odd and a 2-component link if p is even). Since there are no empty bigons in this diagram, $\hat{\partial} = 0$ and

$$2p = \mathrm{rk}\left(\widehat{CFK}(S^3,L)\otimes(\mathbb{F}\oplus\mathbb{F})\right) = \mathrm{rk}\left(\widehat{HFK}(S^3,L)\otimes(\mathbb{F}\oplus\mathbb{F})\right) = 2\det L = 2p',$$

thus $p = p'$. (We conjecture that $q = q'$ is true as well.)

(ii) By Corollary 4.1.6, all perfect diagrams $\mathcal{D}_k$ are close parallel. Let us consider $\mathcal{D}_2$, a $(0,2)$-diagram with only one α-and β-curve each from $\mathcal{D}_k$. $\mathcal{D}_2$ is still perfect; our conclusion follows from part (i). □

Remark 4.4.2. *The above result seems to cast doubt on Conjecture 4.3.1, since the structure of* α*- and* β*-curves in perfect* $(0,k)$*-diagrams is so rigid; only* $O(p^2)$ *distinct configurations up to size* p*. However, note that there are not many restrictions for placing the base points* w_i *and* z_j*, so this intuition may be misleading.*

Bibliography

[1] K. L. Baker, J. E. Grigsby, and M. Hedden. Grid diagrams for lens spaces and combinatorial knot Floer homology. *Int. Math. Res. Not. IMRN*, (10):Art. ID rnm024, 39, 2008.

[2] J. A. Baldwin and W. D. Gillam. Computations of Heegaard-Floer knot homology. *J. Knot Theory Ramifications*, 21(8):1250075, 65, 2012.

[3] D. Bar-Natan, S. Morrison, and et al. The Knot Atlas. *http://katlas.org*, 2014.

[4] S. A. Bleiler and A. C. Jones. On two generator satellite knots. *Geom. Dedicata*, 104:1–14, 2004.

[5] J. C. Cha and C. Livingston. KnotInfo: Table of knot invariants. *http://www.indiana.edu/∼knotinfo*, 2014.

[6] J. H. Conway. An enumeration of knots and links, and some of their algebraic properties. In *Computational Problems in Abstract Algebra (Proc. Conf., Oxford, 1967)*, pages 329–358. Pergamon, Oxford, 1970.

[7] H. Doll. A generalized bridge number for links in 3-manifolds. *Math. Ann.*, 294(4):701–717, 1992.

[8] G. Doyle. Calculating the Knot Floer Homology of (1,1) Knots. *Undergraduate thesis, Princeton University*, 2005.

[9] M. Eisermann. Homological characterization of the unknot. *J. Pure Appl. Algebra*, 177(2):131–157, 2003.

[10] P. Ghiggini. Knot Floer homology detects genus-one fibred knots. *Amer. J. Math.*, 130(5):1151–1169, 2008.

[11] H. Goda, H. Matsuda, and T. Morifuji. Knot Floer homology of $(1, 1)$-knots. *Geom. Dedicata*, 112:197–214, 2005.

[12] C. Gordon and J. Luecke. Knots are determined by their complements. *Journal of the American Mathematical Society*, pages 371–415, 1989.

[13] M. Hedden. Knot Floer homology of Whitehead doubles. *Geom. Topol.*, 11:2277–2338, 2007.

[14] A. Juhász. Holomorphic discs and sutured manifolds. *Algebr. Geom. Topol.*, 6:1429–1457, 2006.

[15] L. H. Kauffman and S. Lambropoulou. Hard unknots and collapsing tangles. In *Introductory lectures on knot theory*, volume 46 of *Ser. Knots Everything*, pages 187–247. World Sci. Publ., Hackensack, NJ, 2012.

[16] E. Klimenko and M. Sakuma. Two-generator discrete subgroups of $\mathrm{Isom}(\mathbf{H}^2)$ containing orientation-reversing elements. *Geom. Dedicata*, 72(3):247–282, 1998.

[17] P. B. Kronheimer and T. S. Mrowka. Gauge theory for embedded surfaces. I. *Topology*, 32(4):773–826, 1993.

[18] C. Kutluhan, Y.-J. Lee, and C. H. Taubes. HF=HM I: Heegaard Floer homology and Seiberg–Witten Floer homology. *arXiv preprint arXiv:1007.1979*, 2010.

[19] W. B. R. Lickorish. *An introduction to knot theory*, volume 175 of *Graduate Texts in Mathematics*. Springer-Verlag, New York, 1997.

[20] R. Lipshitz. A cylindrical reformulation of Heegaard Floer homology. *Geom. Topol.*, 10:955–1097, 2006.

[21] C. Manolescu, P. Ozsváth, and S. Sarkar. A combinatorial description of knot Floer homology. *Ann. of Math. (2)*, 169(2):633–660, 2009.

[22] K. Morimoto, M. Sakuma, and Y. Yokota. Identifying tunnel number one knots. *J. Math. Soc. Japan*, 48(4):667–688, 1996.

[23] Y. Ni. Knot Floer homology detects fibred knots. *Invent. Math.*, 170(3):577–608, 2007.

[24] F. H. Norwood. Every two-generator knot is prime. *Proc. Amer. Math. Soc.*, 86(1):143–147, 1982.

[25] P. Ozsváth, A. I. Stipsicz, and Z. Szabó. Combinatorial heegaard floer homology and nice heegaard diagrams. *Advances in Mathematics*, 231(1):102–171, 2012.

[26] P. Ozsváth and Z. Szabó. Knot Floer homology and the four-ball genus. *Geom. Topol.*, 7:615–639, 2003.

[27] P. Ozsváth and Z. Szabó. Holomorphic disks and genus bounds. *Geom. Topol.*, 8:311–334, 2004.

[28] P. Ozsváth and Z. Szabó. Holomorphic disks and knot invariants. *Adv. Math.*, 186(1):58–116, 2004.

[29] P. Ozsváth and Z. Szabó. Holomorphic disks and topological invariants for closed three-manifolds. *Ann. of Math. (2)*, 159(3):1027–1158, 2004.

[30] P. Ozsváth and Z. Szabó. Heegaard Floer homology and contact structures. *Duke Math. J.*, 129(1):39–61, 2005.

[31] P. Ozsváth and Z. Szabó. An introduction to Heegaard Floer homology. In *Floer homology, gauge theory, and low-dimensional topology*, volume 5 of *Clay Math. Proc.*, pages 3–27. Amer. Math. Soc., Providence, RI, 2006.

[32] J. Rasmussen. Knot polynomials and knot homologies. In *Geometry and topology of manifolds*, volume 47 of *Fields Inst. Commun.*, pages 261–280. Amer. Math. Soc., Providence, RI, 2005.

[33] J. A. Rasmussen. *Floer homology and knot complements*. ProQuest LLC, Ann Arbor, MI, 2003. Thesis (Ph.D.)–Harvard University.

[34] S. Sarkar and J. Wang. An algorithm for computing some Heegaard Floer homologies. *Ann. of Math. (2)*, 171(2):1213–1236, 2010.